TOPICAL REVIEW

Technologies for Energy Storage Power Stations Safety Operation: Battery State Evaluation Survey and a Critical Analysis

**XIANGYANG XIA, JIAHUI YUE [ID], YUAN GUO, CHONGGENG LV,
XIAOYONG ZENG [ID], (Member, IEEE), YONGKAI XIA,
AND GUIQUAN CHEN**

School of Electrical and Information Engineering, Changsha University of Science and Technology, Changsha, Hunan 410114, China

Corresponding author: Xiangyang Xia (307351045@qq.com)

ABSTRACT As large-scale lithium-ion battery energy storage power facilities are built, the issues of safety operations become more complex. The existing difficulties revolve around effective battery health evaluation, cell-to-cell variation evaluation, circulation, and resonance suppression, and more. Based on this, this paper first reviews battery health evaluation methods based on various methods and summarizes the selection of existing health factors in data-driven methods. Secondly, the paper discusses the new research hotspots in the existing battery state evaluation technologies from the perspectives of state evaluation using data fragments and edge computing. Thirdly, we focus and discuss on the safety operation technologies of energy storage stations, including the issues of inconsistency, balancing, circulation, and resonance. To address these issues, we present an intelligent inspection robot, enabling real-time data interaction with the EMS and fulfilling rapid inspection and real-time diagnosis. Above all, we focus on the safety operation challenges for energy storage power stations and give our views and validate them with practical engineering applications, building the foundation of the next-generation techniques that support the development of new power systems.

INDEX TERMS Health factor, state of health, remaining useful life, cell-to-cell variation, entropy, safety operation.

I. INTRODUCTION

Safety control of energy storage batteries, comprehensive safety warnings, and the development of safety systems for energy storage power stations are major directions in the development process of modern electric power systems [1], [2]. The effectiveness and safety of an energy storage power station depend heavily on appropriate monitoring of the battery management system (BMS), with the essential indicators being the state of health (SOH) and remaining useful life (RUL) of the batteries [3], [4], [5], [6].

The degree of degradation of lithium-ion batteries used for energy storage is primarily influenced by external and internal variables. External factors include ambient temperature,

charge/discharge ratio, and discharge depth, while internal factors include the loss of active lithium ions, positive and negative electrode active materials, and electrical conductivity.

Therefore, to achieve accurate evaluation of SOH and RUL, the approaches primarily focus on internal and external characteristic parameters of the battery. These include experiment-based methods, model-based methods, and data-based methods.

(1) Experiment-based methods: evaluating the SOH and RUL of the battery typically involve many experiments and examinations to assess the degree of degradation. Electrochemical impedance spectroscopy (EIS) is utilized to acquire internal parameters such as ohmic internal resistance and polarization capacitance [7], [8], [9], [10]. But it's obvious that the circumstances for direct measurement are harsh and

The associate editor coordinating the review of this manuscript and approving it for publication was Ilaria De Munari [ID].

time-consuming, making them unsuitable for battery management systems.

(2) Model-based methods: rint equivalent circuit model, thevenin equivalent circuit model, second-order RC equivalent circuit model, PNGV equivalent circuit model, GNL equivalent circuit model are examples of modeling methods. At the same time, it employs several adaptive filters, including the extended Kalman filter [11], the H∞ observer [12], and the sliding mode observer [13], to accurately identify the internal characteristic parameters of the equivalent circuit model. Ref. [14] proposed a method for estimation of battery SOH based on a dynamic equivalent circuit model. This method utilizes nonlinear least squares curve fitting to approximate model parameters, capturing dynamic changes in SOH while reducing computational complexity. Ref. [15], in a comparative analysis of equivalent circuit models of different orders, was found that for lithium-iron batteries, the first-order and second-order models yield better simulation results. Ref. [16] introduced a multi-time scale edge-level equivalent circuit model.

(3) Data-based methods: these methods for evaluating battery health state do not require in-depth modeling and research of the intricate deterioration process. And these methods skip the complex calculation process of identifying the internal features of the battery and are not restricted to a specific battery's type [17], [18], [19]. The major components include data preprocessing and the selecting efficient health factors (HFs) for evaluation. According to the operational regulations of energy storage power stations, the operation conditions of batteries mainly involve constant current (CC)/constant voltage (CV) charging and discharging processes. Based on the above charging and discharging processes, some scholars focus on the extraction of health features, such as the amount of capacity change, energy change, voltage change, current change, time change, and secondary processing of the above data. For example, Ref. [20] predicted the SOH and RUL of lithium-ion batteries using voltage changes at different time intervals during the CC charging process and current changes at different time intervals during the CV charging process as health factors. Ref. [21] selected the time required for a voltage increase segment during the CC charging stage, the time required for a current reduction segment during the CV charging time stage, and the number of cycles as health features to predict the RUL. Ref. [22] chose 12 health factors, including charging time and its CC/CV ratio, integration of current and temperature curves, and maximum slope between CV and CC curves. References [23], [24], and [25] calculated the first derivative of the voltage-capacity relationship to draw the capacity increment curve V-dQ/dV, and extracted important feature points of the curve as health factors to evaluate SOH. Above all, precisely identifying health indicators that can describe battery aging is critical. This paper describes the extraction of health-related parameters.

While summarizing the health evaluation methods, this paper discusses the new research hotspots in the existing battery state evaluation technologies.

(1) State evaluation using data fragments: a series of health factors from the charging or discharging curve have been extracted. These variables are then associated with the state of the batteries using machine learning methods. However, in practice, batteries are rarely fully charged or depleted, and only a portion of random charging or discharging data is collected. As a result, predicting the state using random data segments has become an essential problem that must be addressed.

(2) Edge computing: as large-scale energy storage power plants are built, battery monitoring data has expanded dramatically. To solve this, the development of an edge computing platform for energy storage batteries has started. However, existing edge platforms primarily monitor the external characteristics of batteries and do not focus on monitoring internal characteristics, causing a certain degree of deviation in the health state evaluation. Therefore, there is a need for more advanced edge computing platforms that can enable real-time monitoring of both internal and external battery parameters, allowing for more precise evaluation.

As energy storage devices are incorporated into the power grid, inconsistency, balancing, circulation, and resonance must be considered while achieving effective battery state evaluation.

The initial performance of batteries may vary during the manufacturing and production stages. Furthermore, differing operating environments might worsen inconsistencies, even after grouping. As a result, efficient monitoring of cell-to-cell variance is essential and cannot be overlooked [26]. Ref. [27] provided a data-driven weighted scoring mechanism based on fluctuations in voltage, temperature, internal resistance, capacity, and electric amount. Ref. [28] analyzed cell-to-cell inconsistencies utilizing current, temperature, and age. In Ref. [29], capacity, open-circuit voltage, and ohmic resistance were used to assess battery inconsistency using the standard deviation coefficient. To improve the inconsistent evaluation indicators, this paper proposes including the idea of information entropy in the effective evaluation of the balance of batteries in an energy storage station. This is performed by selecting appropriate operating segment data to generate the characteristic data set for batteries. Then, the entropy value of the aforementioned characteristic data is used to analyze cell-to-cell variance.

When energy storage devices are more fully incorporated into the power system, their interactions with the grid must be considered. The use of multiple converters in energy storage systems has increased the risk of circulation and resonance. This results in substantial conflicting objectives between the power grid and energy storage systems.

Above all, this article proposes the use of intelligent inspection robots in storage power stations to efficiently evaluate inconsistency, circulation, and resonance. They

TABLE 1. List of acronyms and abbreviations.

Acronym	Description
BMS	Battery Management System
BP	Back Propagation Neural Network
CC	constant current
CNN	Convolutional Neural Networks
CV	constant voltage
EFM	Empirical Fitting Mode
EIS	Electrochemical Impedance Spectroscopy
ELM	Extreme Learning Machines
EMS	Energy Management System
GNL	General Nonlinear Model
GPR	Gaussian Process Regression
HFs	Health Factors
ICA	Incremental Capacity Analysis
LSTM	Long Short-term Memory
MAE	Mean Absolute Error
MAPE	Mean Absolute Percentage Error
MLM	Machine Learning Model
NANN	Nonlinear Autoregressive Neural Networks
NASA	National Aeronautics and Space Administration
PNGV	Partnership for a New Generation of Vehicles
PC	Personal Computer
RMSE	Root Mean Square Error
RUL	Remaining Useful Life
SOC	State of Charge
SOH	State of Health
SVR	Support Vector Regression

enable online monitoring of the connection condition of battery packs, as well as the wear and tear of cables and insulation, delivering critical operational data to facilities and ensuring the effectiveness of subsequent analysis and decision-making. At the same time, the intelligent inspection robot can communicate with the EMS to enable dynamic data interaction, resulting in speedy inspection and real-time detection of inconsistency, circulation, and resonance. Furthermore, using machine learning and artificial intelligence technologies, intelligent inspection robots can gradually learn and increase their inspection efficiency and accuracy. Above all, precisely identifying health indicators that can describe battery aging is critical. This study describes the extraction of health-related parameters.

Faced with the highly challenging issues mentioned above, this paper is structured as follows: Section II reviews state evaluation methods from three perspectives: EIS, equivalent circuit models, and data-driven methods. We also summarize the selection of health factors in data-driven methods. Section III highlights new research hotspots in battery state evaluation, specifically state evaluation using data fragments and edge computing. Section IV focuses on the safety operating technologies of energy storage stations, such as inconsistency, balance, circulation, and resonance, and proposes an intelligent inspection robot to address these difficulties. Finally, Section V summarizes the main conclusions. For the reader's convenience, Tab. 1 lists all the acronyms used in this article.

II. DISCUSSION ON THE BATTERY STATE EVALUATION METHODS

A. ELECTROCHEMICAL IMPEDANCE SPECTROSCOPY
To generate the current response signal, a sinusoidal voltage signal is injected into the electrode [30], [31]. The impedance
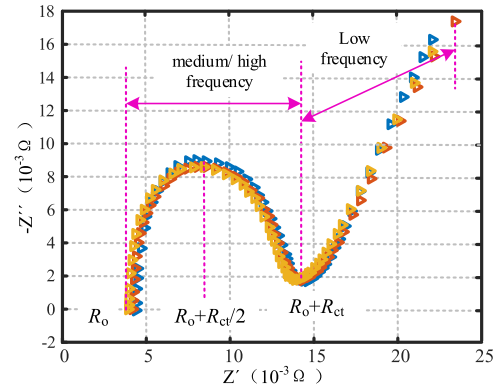

FIGURE 1. The results of impedance measure.

of the battery at that frequency can be determined by calculating the ratio of excitation voltage to response current. This can be expressed as:

$$Z(j\omega) = E(j\omega) / I(j\omega) \tag{1}$$

The impedance of the electrode can be calculated from these signals, which can reveal the essence of the degrading mechanism, as shown in Fig. 1.
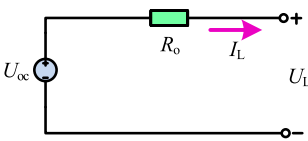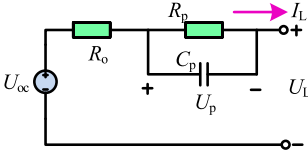
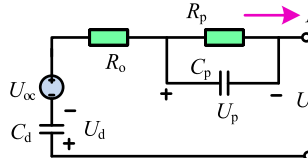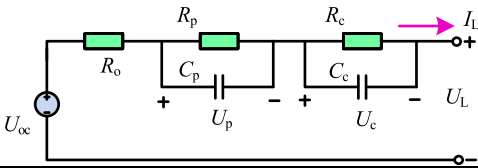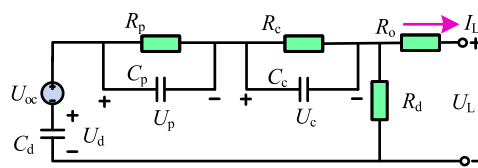### B. BATTERY EQUIVAIENT CIRCUIT MODEL
The equivalent circuit model is a powerful tool for modeling the behavior of lithium-ion batteries. By using a linear variable parameter circuit model, this approach can simulate the non-linear running characteristics of batteries with high accuracy and computational efficiency [32], [33]. There are several types of equivalent circuit models available [34], [35], [36], including the Rint, Thevenin, PNGV, second-order RC, and GNL models. The description equations and model parameters are shown in the Tab. 2.

Among the various equivalent circuit models, the Rint model is the simplest, but it has the poorest simulation accuracy. The Thevenin and PNGV models are first-order equivalent circuit models with relatively simple structures that are practical for engineering applications. However, their use is limited to CC/CV charge/discharge running conditions. For the PNGV model, serially connecting capacitors will result in a certain degree of calculation error. In contrast, the second-order RC model and the GNL model are more complex second-order equivalent circuits that can capture electrochemical polarization impedance and concentration effects, but the difficult building in model and the huge computation work are obvious.

C. DATA-DRIVEN METHODS
After filtering attribute data and constructing health factors as inputs to the model algorithm, the selection of an appropriate machine learning algorithm is critical. Popular options include support vector regression (SVR), Gaussian process regression (GPR), long short-term memory (LSTM),

TABLE 2. Comparison among the commonly used battery models.

Model	Descriptive equations	Descriptive equations
Rint		$U_L = U_{oc} - I_L R_o$
Thevenin		$U_{oc} = U_L + I_L R_o + U_p$ $\dfrac{dU_p}{dt} = \dfrac{I_L}{C_p} + \dfrac{U_p}{R_p C_p}$
PNGV		$U_L = U_{oc} - I_L R_o - U_p - U_d$ $\dfrac{dU_p}{dt} = \dfrac{I_L}{C_p} + \dfrac{U_p}{R_p C_p}$ $\dfrac{dU_d}{dt} = \dfrac{I_L}{C_d}$
Second-order RC model		$U_L = U_{oc} - U_p - U_c - I_L R$ $\dfrac{dU_p}{dt} = \dfrac{I_L}{C_p} + \dfrac{U_p}{R_p C_p}$ $\dfrac{dU_c}{dt} = \dfrac{I_L}{C_c} + \dfrac{U_c}{R_c C_c}$
GNL		$U_L = U_{oc} - I_L R_o - U_p - U_c - U_d$ $\dfrac{dU_d}{dt} = \dfrac{I_L}{C_d} + \dfrac{U_{oc}}{R_d C_d} - \dfrac{U_d}{R_d C_d} - \dfrac{U_p}{R_d C_d} - \dfrac{U_c}{R_d C_d}$ $\dfrac{dU_p}{dt} = \dfrac{I_L}{C_p} + \dfrac{U_{oc}}{R_d C_p} - \dfrac{U_d}{R_d C_p} - \dfrac{U_p}{R_d C_p} - \dfrac{U_c}{R_d C_p} - \dfrac{U_p}{R_p C_p}$ $\dfrac{dU_c}{dt} = \dfrac{I_L}{C_c} + \dfrac{U_{oc}}{R_d C_c} - \dfrac{U_d}{R_d C_c} - \dfrac{U_p}{R_d C_c} - \dfrac{U_c}{R_d C_c} - \dfrac{U_c}{R_c C_c}$

extreme learning machine (ELM), neural networks (NN), among others.

1) SUPPORT VECTOR REGRESSION

The Support Vector Regression (SVR) model is designed to address nonlinear regression problems by mapping them from a low-dimensional feature space to a higher-dimensional space. It transforms the problem into a linear regression task. Additionally, the SVR model can generate regression models by estimating the model parameters using small data samples.

For the training sample set $D = \{(x_1, S_{SOH}^1), (x_2, S_{SOH}^2), (x_3, S_{SOH}^3), \ldots, (x_n, S_{SOH}^n)\}$, the lithium-ion battery SOH model is:

$$f(x) = w^T x + b \qquad (2)$$

where w is the weight value; b is the bias.

If the tolerance deviation is ε, the loss value will be calculated when the absolute deviation between $f(x)$ and SOH is greater than it. As a result, the support vector regression model parameters can be calculated as follows:

$$
\begin{cases}
\min\limits_{\omega, b} : \dfrac{1}{2} \|\omega\|^2 + C \sum\limits_{i=1}^{n} L_\varepsilon \left(S_{SOH}^i - f(x_i) \right) \\
L_\varepsilon (f(x), S_{SOH}) = \begin{cases} 0, & |S_{SOH} - f(x)| \le \varepsilon \\ |S_{SOH} - f(x)| - \varepsilon, & \\ & |S_{SOH} - f(x)| > \varepsilon \end{cases}
\end{cases} \qquad (3)
$$

where C is the penalty factor; $L_\varepsilon(\cdot)$ is the loss function; n is the number of the training sample.

In Ref. [37], the SVR model was integrated with novel voltage-capacity-model-based ICA methods to accurately predict battery SOH. Ref. [38] used the enhanced ant-lion optimization technique to optimize support vector regression, allowing for effective SOH evaluation. Furthermore, Ref. [39] integrated SVR with lithium-ion battery surface temperature to forecast SOH, resulting in lower computing costs and increased robustness.

2) GAUSSIAN PROCESS REGRESSION

The Gaussian Process Regression (GPR) model is characterized by its generalization and analytical properties. To train

the Gaussian process parameters, eigenvectors and health factors SOH(X, S_{SOH}) are utilized. Subsequently, the current eigenvectors are used to determine the posterior probability distribution, which is used to evaluate the SOH of lithium-ion battery and provide a confidence interval. The regression calculation equations are as follows:

$$\begin{cases} \begin{bmatrix} S_{SOH} \\ S_{SOH}^* \end{bmatrix} \sim N \left(0, \begin{bmatrix} \kappa_f\,(X,X) + \sigma_n^2 I & \kappa_f\,(X,X^*) \\ \kappa_f\,(X,X^*)^T & \kappa_f\,(X^*,X^*) \end{bmatrix} \right) \\ p\left(S_{SOH}^* \middle| X, S_{SOH}, X^*\right) = N\left(S_{SOH}^* \middle| \bar{S}_{SOH}^*\,, cov\left(S_{SOH}^*\right)\right) \\ \kappa_f\,(X,X) = \left(\sigma_f^2 e^{\left(-(X_i-X_j)^2 \middle/ 2\lambda^2\right)}\right)_{n \times n} \end{cases}$$

(4)

where σ_n^2 is the noise covariance matric; σ_f and λ are the core parameters of the Gaussian process regression model, obtaining using training data; $N(\cdot)$ is the normal distribution function; $\bar{S}_{SOH}^*$ and $cov\left(S_{SOH}^*\right)$ are the mean and variance of the SOH.

In Ref. [40], the GPR model was integrated with a neural network to assess and forecast battery SOH. Ref. [41] used differential thermal voltammetry and the SVR model to predict battery health. Furthermore, Ref. [42] updated the measurement of input variable information and covariance function design in the Gaussian process regression model, resulting in an improved method for evaluating battery SOH.

3) LONG SHORT-TERM MEMORY

The Long Short-term Memory (LSTM) model incorporates a gating mechanism that consists of a forgetting gate, an input gate, and an output gate. The forgetting gate determines the degree to which the higher-level unit retains previous information. Meanwhile, the input gate, combined with an activation function, regulates the amount of new information that is allowed to enter the unit and updates its internal state accordingly. Finally, the output gate governs the extent to which the unit's output is filtered before being passed on to the next layer. The calculation process at time t is:

$$\begin{cases} f_t = \sigma(W_f \cdot x_t + U_f \cdot h_{t-1} + b_f) \\ i_t = \sigma(W_i \cdot x_t + U_i \cdot h_{t-1} + b_i) \\ \tilde{C}_t = \tanh(W_c \cdot x_t + U_c \cdot h_{t-1} + b_c) \\ C_t = f_t \cdot C_{t-1} + i_t \cdot \tilde{C}_t \\ O_t = \sigma(W_o \cdot x_t + U_o \cdot h_{t-1} + b_o) \\ h_t = O_t * \tanh(C_t) \end{cases}$$

(5)

where f_t, i_t, O_t are the results for three types of gates; W_f, W_i, W_c, W_o, U_f, U_i, U_c, U_o are the weight matrix; b_f, b_i, b_c, b_o are the bias vector; $\sigma(\cdot)$ and $\tanh(\cdot)$ are the activation functions.

As noted in Ref. [43], LSTM-based SOH evaluation surpasses nonlinear autoregressive neural networks and convolutional neural networks. Ref. [44] introduced a multi-layer LSTM algorithm with an attention mechanism that extracts aging information from data segments and accurately predicts SOH. In Ref. [45], the LSTM model was integrated with the

continuous and discrete wavelet transforms to evaluate SOH. In Ref. [46], the differential enhanced gray wolf optimizer was utilized to optimize the hyperparameter selection of the LSTM model for accurate SOH prediction.

4) EXTREME LEARNING MACHINE

The Extreme Learning Machines (ELM) model is a non-iterative learning algorithm that does not require any iterative phases for determining network parameters. This approach significantly reduces the time needed to train the network, making it faster than traditional learning algorithms, while still achieving high accuracy. The output of the model is as follows:

$$y = \sum_{j=1}^{m} \phi_{j,k} \cdot g\left(\sum_{i=1}^{n} \omega_{i,j}x_i + b_i\right)$$

(6)

where $g(\cdot)$ is the activation functions; $\omega_{i,j}$ and b_j are the input-weights and bias; $\phi_{j,k}$ is the output-weights.

In Ref. [47], a battery health state evaluation model was developed using regularized ELM to address the issue of overfitting. Ref. [48] optimized the regularized ELM algorithm using conjugate gradient, resulting in reliable evaluation of the battery's operating states. Ref. [49] optimized an ELM model using variable forgetting factors for online prediction of Li-ion battery SOH.

5) BACK PROPAGATION NEURAL NETWORK

The BP model, which captures the mapping relationship between inputs and outputs, is typically composed of input layers, hidden layers, and output layers. This model possesses strong self-organizing and self-learning capabilities, as well as a high degree of flexibility, making it well-suited for addressing the nonlinear problem of SOH evaluation for lithium-ion batteries. The output of the model is as follows:

$$\begin{cases} Z = \omega^T \cdot X + b \\ a = \sigma(Z) \end{cases}$$

(7)

where X is the input; ω is the connection weight; b is bias; $\sigma(\cdot)$ is activation functions; a is the predicted value.

Assuming y as the actual value, the loss function as $L(a,y)$ and the partial derivative of the cost function is:

$$\begin{cases} \dfrac{\partial L\,(a,y)}{\partial \omega} = \dfrac{\partial L\,(a,y)}{\partial a} \cdot \dfrac{\partial a}{\partial Z} \cdot \dfrac{\partial Z}{\partial \omega} \\ \dfrac{\partial L\,(a,y)}{\partial b} = \dfrac{\partial L\,(a,y)}{\partial a} \cdot \dfrac{\partial a}{\partial Z} \cdot \dfrac{\partial Z}{\partial b} \end{cases}$$

(8)

Based on the above equations, the weights and thresholds of each layer are updated using the gradient descent error back-propagation method. Through continuous iteration and updating, the loss function $L(a,y)$ is minimized to obtain the optimal prediction value.

In Ref. [50], the impact of varying ambient temperatures was incorporated into the BP neural network for predicting the SOH of batteries. In Ref. [51], the simulated annealing-back propagation model was proposed, which achieves for

online estimation of the long-term SOH of batteries. Ref. [52] proposed a SOH evaluation method based on the BP neural network optimized by a genetic algorithm and the fixed characteristic voltage interval.

6) HYBRID MODELS

Due to the limitations of individual methods, such as low prediction accuracy and poor generalization, hybrid models have emerged as a research focus for improving the accuracy and stability of prediction results. By combining multiple methods, these models can leverage the strengths of each component to achieve better performance than any single method alone.

Hybrid models can be broadly classified into two categories, as shown in Fig. 3, those driven by equivalent circuit methods and data-driven methods, and those driven by multiple data-driven methods. The former approach typically involves combining the physical insights provided by equivalent circuit models with the flexibility of data-driven methods to achieve accurate predictions. The latter approach, on the other hand, involves integrating multiple data-driven models to enhance the overall performance of the hybrid model.

The output of the model is as follows:

$$\begin{aligned} SOH = {} & \omega_1^* \cdot \text{soh\_predict}\,(Y_1) + \omega_2^* \cdot \text{soh\_predict}\,(Y_2) \\ & + \omega_3^* \cdot \text{soh\_predict}\,(Y_3) + + \omega_4^* \cdot \text{soh\_predict}\,(Y_4) \end{aligned}$$

(9)

where Y_i is the input of each model; $\text{soh\_predict}\,(Y_i)$ is the predicted result of the health state through the i_{th}-method; ω_1^*, ω_2^*, ω_3^*, ω_4^* are output the weights of the results separately, $\omega_1^* + \omega_2^* + \omega_3^* + \omega_4^* = 1$.

Ref. [53] proposed a prediction model that combined the capacity decay model and the internal resistance growth models. In Ref. [54], the unscented particle filter was integrated with an enhanced multiple kernel relevance vector machine method to create a battery state prediction model. Ref. [55] suggested a battery state prediction model using an LSTM network and a GPR model. Ref. [56] suggested a hybrid data-driven strategy that integrates ELM and a random vector functional link neural network to extract the relationship between the specified health parameters and SOH.

D. HEALTH FACTORS

Health factors (HFs) can be used to assess the SOH of lithium-ion batteries based on operational data and to develop accurate predictive models. Since it is challenging to evaluate SOH of batteries in real-time, it is crucial to identify the HFs that are strongly correlated with capacity and can effectively characterize degradation.

1) INCREMENTAL CAPACITY ANALYSIS

The capacity increment (IC) curve is obtained by combining battery's capacity and terminal voltage data. The principle behind this is to generate a terminal voltage-capacity (V-Q) curve under constant current charging or discharging conditions and then calculate the first derivative of the V-Q curve to obtain the capacity increment curve V-dQ/dV. The incremental capacity analysis (ICA) method is developed based on this curve. As shown in Fig. 3, certain health factors, such as peak height and peak position, can be derived from the V-dQ/dV curve. By monitoring changes in these parameters, which accurately reflect the degree of deterioration, battery's health can be examined and managed effectively [55], [57], [58].

2) VOLTAGE

Based on the constant current charging process, this process can be divided into several segments: the discharge initial segment, the discharge stable segment, the discharge end segment, and the discharge recovery segment. Each voltage segment exhibits certain health characteristics.

Fig. 4 shows the sharp voltage drop that occurs during the discharge process. The sharp voltage drop is mainly caused by the ohmic resistance. As the battery ages, this resistance gradually increases, leading to a obvious voltage drop.

Focusing on the amplitude of the stable voltage drop during the discharge process, it is worth noting that this voltage drop is mainly caused by the polarization resistance. As the battery ages, the amplitude of the voltage drop gradually increases, as shown in Fig. 5. Therefore, the amplitude of the voltage drop can be used as a health factor to evaluate the health state of the battery [59].

Based on the constant current charging process, the time required to charge the battery to the cut-off voltage decreases as the battery ages. Therefore, as shown in Fig. 6, a specific voltage segment change rate can be used as a health factor.

3) CURRENT

The time required to charge the cut-off current decreases as the battery ages. Therefore, as seen in Fig. 7, a specific current segment change rate can be used as a health factor to assess battery aging.

4) CHARGING/DISCHARGING TIME

Constant current charge time (CCCT) and constant current discharge time (CCDT) are commonly used indexes that are closely related to battery's capacity.

As shown in Fig. 8, the charging or discharging time required for the constant current procedure decreases significantly as the battery degrades over time, which can be regarded as health factors [60].

The time required for the battery to reach its maximum temperature during the charging process decreases rapidly as the ohmic internal resistance and polarization resistance increase with battery aging. As a result, as shown in the figure below, the time required to reach the maximum temperature of the battery can be used as a health factor to assess degradation.

5) TEMPERATURE

During the charging or discharging process, the battery gradually ages and degrades, leading to an increase in both the ohmic internal resistance and the polarization internal
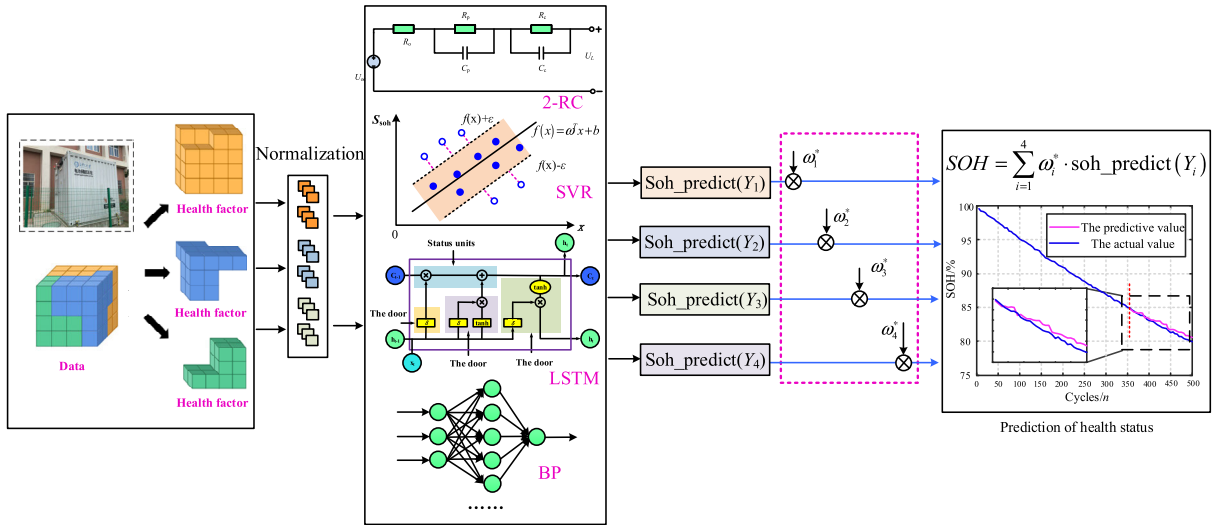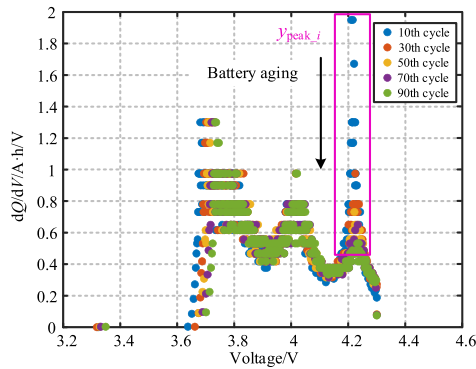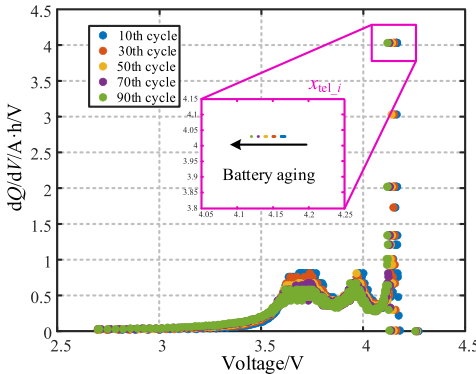
FIGURE 2. The structure of hybrid models.

a) Peak variation of the incremental capacity curve during charging

b) Position variation of the incremental capacity curve during discharging

FIGURE 3. The change trend of incremental capacity curve.

FIGURE 4. The change trend of sharp voltage drop.
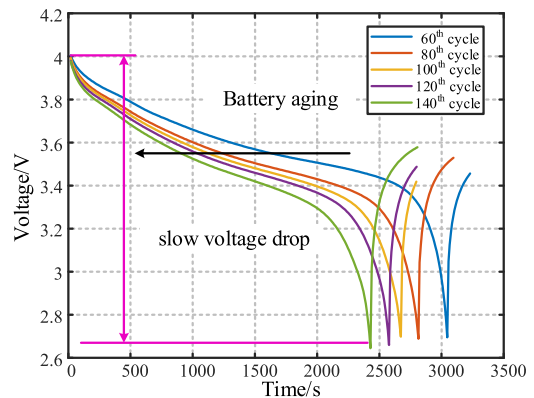
FIGURE 5. Fig.4 The change trend of slow voltage drop.

resistance, as well as a rise in the maximum temperature. As shown in Fig. 10, the highest temperature during the charging or discharging process can be used as a health factor to assess degradation.

As the battery ages, its temperature gradually increases. Therefore, as shown in Fig. 11, a specific temperature segment change rate can be used as a health factor to assess battery aging.
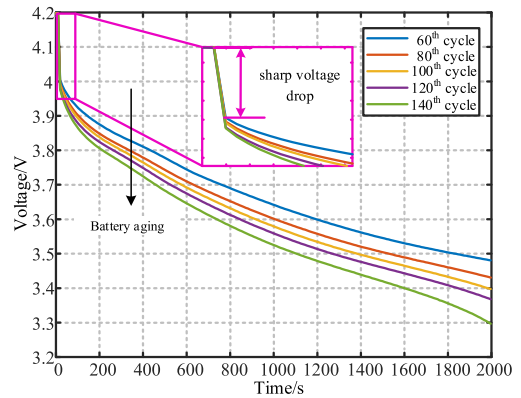
6) SUMMARIZATION

In summary, the health factors have been reviewed, and the practical implementation and their real-world effectiveness of these factors for prediction SOH and RUL in the references is provided in Tab. 3.

At the same time, it is important to note that the selection of different health factors is related to the operational conditions, service life and other factors of the energy storage station.

TABLE 3. A synopsis of the reviewing results for the Health factors.

| Object	Ref.	HFs	Evaluation precision
INCREMENTAL CAPACITY ANALYSIS	[62]	The peak position of the IC curve and the area under the peak	RMSE<0.4
	[63]	The peak position and valley position of the IC curve	maximum errors<2.5%
	[64]	The peak position of the IC curve	RMSE<1.33%;RMSE<2.92% (different data sets)
VOLTAGE	[65]	The value of the voltage interval on the left and right sides of the IC curve peak	errors<2.5%
	[66]	The terminal voltage curves of the battery under different cycle numbers during charge process	errors<5%
	[67]	The value of the mean voltage falloff during the discharging period	AEs<5
	[68]	The value of voltage increase after reaching 3.9V in CC charging process	Average RMSE =1.23%
	[69]	The area under the voltage curve at each cycle	MAE、RMSE<1.5%
CURRENT	[70]	The change value of the charging current in the CV stage	MAE<2.2%
	[71]	The current reduction after entering CV charging process	MAPE<1.2 %
CHARGING/DISCHARGING TIME	[72]	The time required to the peak temperature during charging process	RMSE=0.73% MAXE=2.3%
	[73]	The charging duration sequence of the continuous equal voltage interval during the CC charging process	RMSE<1.76%
	[74]	The time interval of an equal charging/discharging voltage difference	MSPE<1.64%
	[75]	The charging time from 3.8V to 4.1V of the battery.	MAPE<0.67%; RMSE<1.17%
TEMPERATURE	[76]	The changing rate of temperature from the discharging data	RE<5.36%
	[77]	The discharge temperature curve in the time integral	Average maximum absolute errors<2.88%
	[78]	The surface temperature from 1000s to the end of discharge	error<4.12%
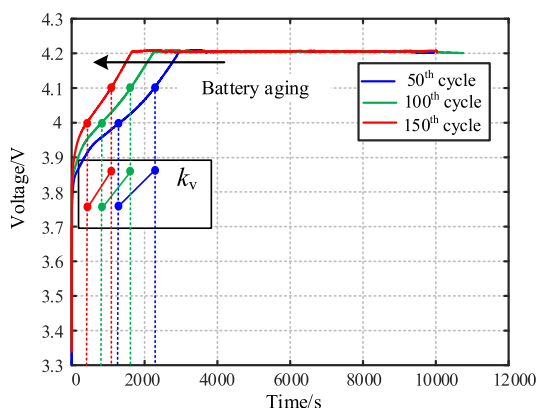
FIGURE 6. The change rate of voltage.

FIGURE 7. The change rate of current.

a) The change of constant current charging time

b) The change of constant current discharge time

FIGURE 8. The change trend of constant current charging and discharging time.
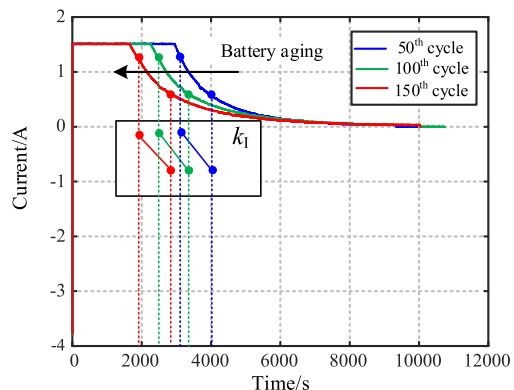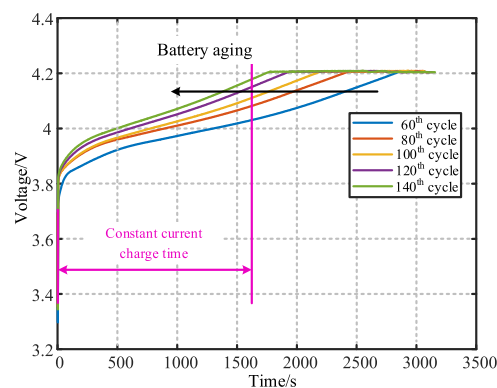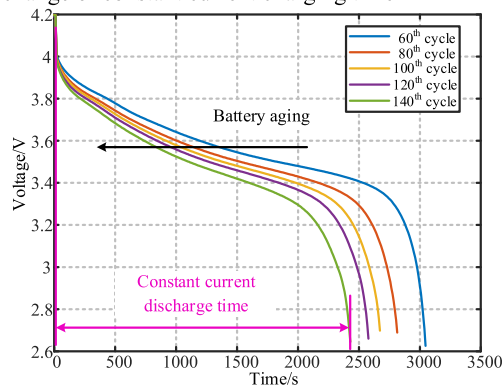
III. NEW TECHNOLOGIES FOR BATTERY STATE EVALUATION

A. BATTERY STATE EVALUATION USING DATA FRAGMENTS

In actual applications, operational data for batteries is sometimes insufficient, making it difficult to gain a true depiction of their performance [78], [79]. Therefore, many scholars estimate the battery state using data segments, as shown in the Tab. 4.

Based on the current research status, this paper proposes two methods for evaluating capacity from the perspectives of Empirical Fitting Model (EFM) and Machine Learning Model (MLM).

TABLE 4. A synopsis of the reviewing results for evaluation the battery state using data segments.

| Ref.	Objects	Description of experiment data
[81]	The charge capacity curve with respect to the voltage of batteries	Sandia National Lab
[82]	The partial charging data from the constant current stage	--
[83]	The partial data from the CV charging stage	--
[84]	The CC charging data that fall within the partial charging voltage range	The center for Advanced Life cycle Engineering at the University of Maryland, which contains several LiCoO2 batteries and Sandia National Labs.
[85]	The available partial charging voltage (the OCV-SOC measured at 1/20C under 25°C)	The NASA data set and the Oxford data set
[86]	The partial charging voltage data	--
[87]	The random charging voltage data	The NASA data set and the Oxford data set
[88]	The partial incremental capacity curve data	The NASA data set and the Calce data set
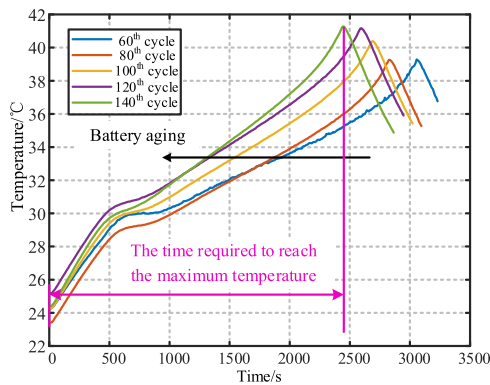
FIGURE 9. The change trend of time required to reach the maximum temperature.
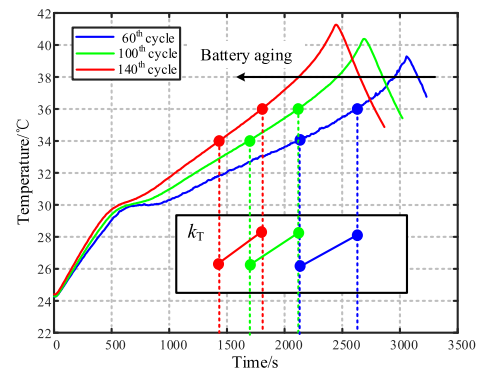

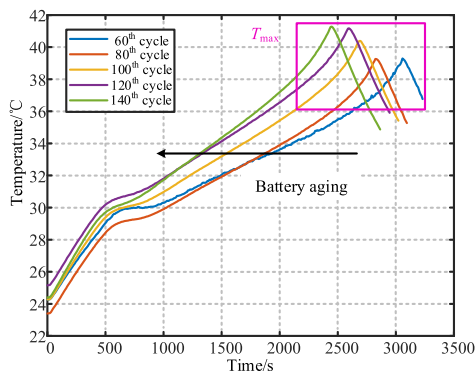
FIGURE 11. The change rate of temperature.

FIGURE 10. The change trend of maximum temperature.

- EFM: the whole historical data contains crucial information, such as a sharp rise in voltage during constant current charging, which indirectly reflects the battery's ohmic internal resistance. An empirical fitting model of sharp voltage rise $\{\Delta u_1, \Delta u_2, \ldots, \Delta u_k\}$ and the related capacity $\{c_1, c_2, \ldots, c_k\}$ can be built by fitting a large amount of historical data, as shown in Fig. 12. If the existing fragmented data contains this feature, the magnitude of the sharp voltage rise can be incorporated into the empirical model to estimate the battery's capacity, resulting in state evaluation.

- MLM: this method constructs CNN-LSTM models for different voltage segments based on a large number

of historical data sets. Taking charging voltage as an example, we construct the data sets for different voltage ranges, specifically 3.8 V to 3.9 V, 3.9 V to 4.0 V, 4.0 V to 4.1 V, and 4.1 V to 4.2 V. From the historical data sets of the aforementioned voltage range, we extract the health factors $\{HF_1, HF_2, \ldots, HF_k\}$ and their corresponding remaining capacities $\{c_1, c_2, \ldots, c_k\}$, and construct CNN-LSTM models for different voltage ranges. Then, the existing fragmented data is completed to the voltage interval that contains the highest amount of the above fragmented data, using the nonlinear fitting curve. And we extract health factors $\{HF_1, HF_2, \ldots, HF_m\}$ from the above completed voltage data. The structure is illustrated in Fig. 13. Finally, we incorporate these health factors into the CNN-LSTM model of the corresponding voltage range to achieve capacity prediction, achieving the state evaluation.

To demonstrate the effectiveness of the proposed EFM, we focus on B0006 of NASA's publicly available lithium-ion battery aging data, which contains critical information on the magnitude of the sharp voltage rise during the 140th cycle. This paper develops a nonlinear fitting model $c(\Delta u)$ based on the sharp voltage rise from the 55th to 139th cycles and the corresponding capacity. The functional connection is expressed as Eq. 10, allowing for a direct evaluation of the remaining capacity for the 140th cycle. The result is displayed
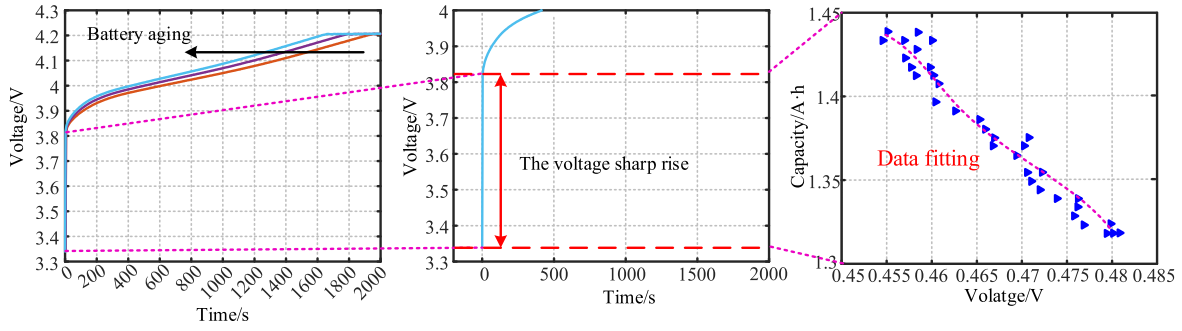
FIGURE 12. Diagram of the proposed prediction health state based on empirical modeling.

a) Prediction health state based on the current interval

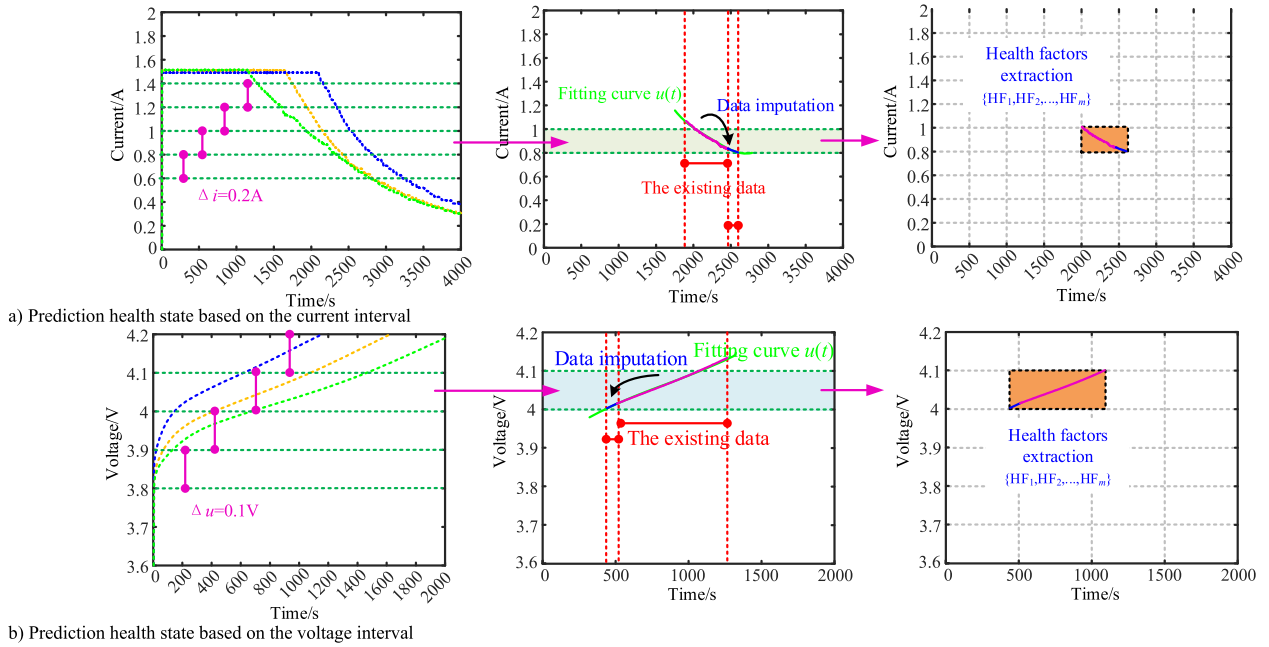b) Prediction health state based on the voltage interval

FIGURE 13. Diagram of the proposed prediction remaining life based on machine learning model.

in Tab 4.

$$c(\Delta u) = 10.03 \cdot \Delta u^2 + 39340 \cdot e^{(-34.81 \cdot \Delta u)} \qquad (10)$$

To demonstrate the effectiveness of the proposed MLM, we focus on B0007 of NASA's publicly available lithium-ion battery aging data, which the voltage fragment data in the voltage range of 4.01V to 4.11V for the 114th cycle is known.

Firstly, the voltage change rates kv_1 from 4.0 V to 4.05 V and kv_2 from 4.05 V to 4.1 V are chosen as health factors. Based on the historical battery aging data of NASA, a large number of health factors historical data sets $\{k_{v1\_1}^*, k_{v1\_2}^*, k_{v1\_3}^*, \ldots, k_{v1\_k}^*\}$, $\{k_{v2\_1}^*, k_{v2\_2}^*, k_{v2\_3}^*, \ldots, k_{v2\_k}^*\}$, as well as corresponding remaining capacities $\{c_1, c_2, \ldots, c_k\}$, are obtained, and then a CNN-LSTM model for the voltage range of 4.0 V to 4.1 V is constructed.

Then, using fragmentation data from the voltage range of 4.01 V to 4.11 V, a nonlinear fitting model $u(t)$ is constructed, as seen in Eq. 11.

$$u(t) = -722.1 \cdot t^2 + 224.5 \cdot e^{(0.9903 \cdot t)} \qquad (11)$$
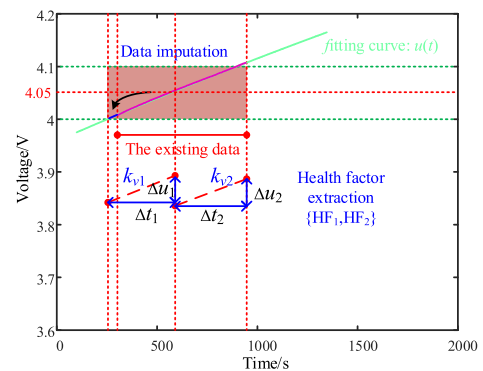

FIGURE 14. Schematic diagram of segmented modeling for B0006.

And the data of the voltage range from 4.0V to 4.01V is completed through the above model, that is, the complete voltage data of the voltage range from 4.0V to 4.1V is constructed.

The voltage change rate k_{v1} from 4.0 V to 4.05 V and the voltage change rate k_{v2} from 4.05 V to 4.1 V are selected
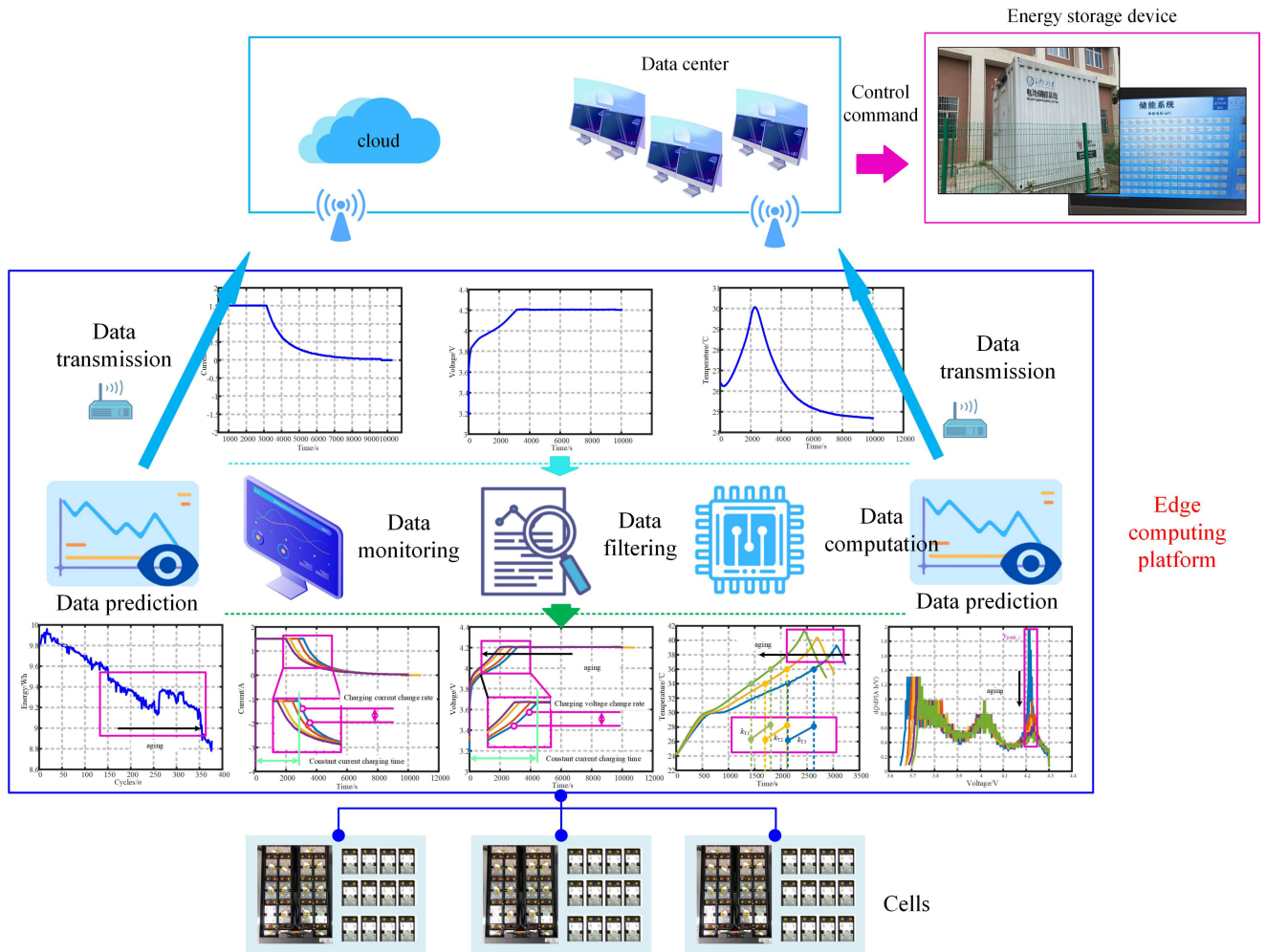
FIGURE 15. The structure of cloud platform.

TABLE 5. Statistical results of capacity evaluation error.

Method	No.	The actual value/A·h	Prediction/A·h	MAE/A·h
Empirical Fitting Model	B0006	1.4618	1.4866	0.0249
Machine Learning Model	B0007	1.3786	1.3632	0.0154

as the health factors of the fragmented data,, as illustrate in Fig. 14.

Finally, the health factors $\{k_{v1}, k_{v2}\}$ are incorporated into the corresponding voltage range of the CNN-LSTM model to predict the remaining capacity at the 114th cycle. The result serves as the previous moment output for the RBF-ARX model, enabling the estimation remaining capacity for subsequent cycles. The result is shown in the Tab. 5.

As shown in the above table, the MAE of predicted remaining capacity based on data fragments proposed in this paper is at a low level, demonstrating the effectiveness of the proposed methods.

Meanwhile, in the face of limited and random data, different optimization algorithms can be employed to effectively

supplement the data, thereby achieving the extraction of health factors.

B. EDGE COMPUTING

Edge computing is a key technology for addressing the safety challenges of energy storage batteries [87], [88], [89]. Specifically, edge computing involves computation and data processing, realizing more efficient battery management and optimization, as shown in Fig. 15. Compared to traditional cloud computing, edge computing transmits the data after being calculated, while the data is encrypted using communication protocols, and offers higher real-time performance and lower latency, making it a promising solution for practical applications in energy storage.

This article proposes a battery health management edge computing platform of energy storage power station. It establishes information communication between the batteries and BMS, enabling transmission of real-time operational data.

Compared to other edge computing platforms that monitor the external characteristics like current, voltage, and temperature, the edge computing platform proposed in this paper
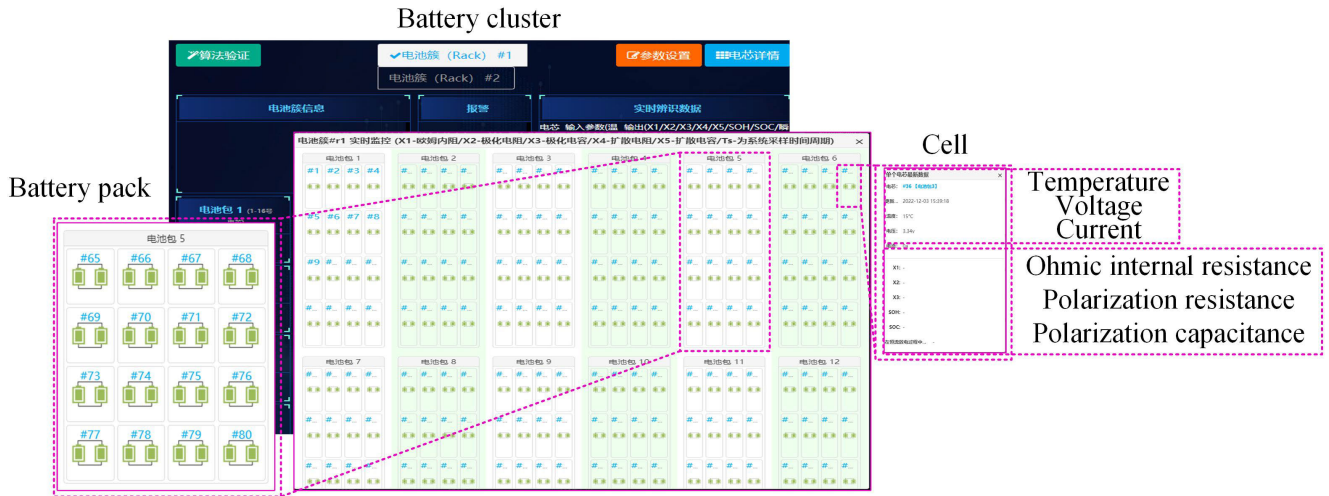
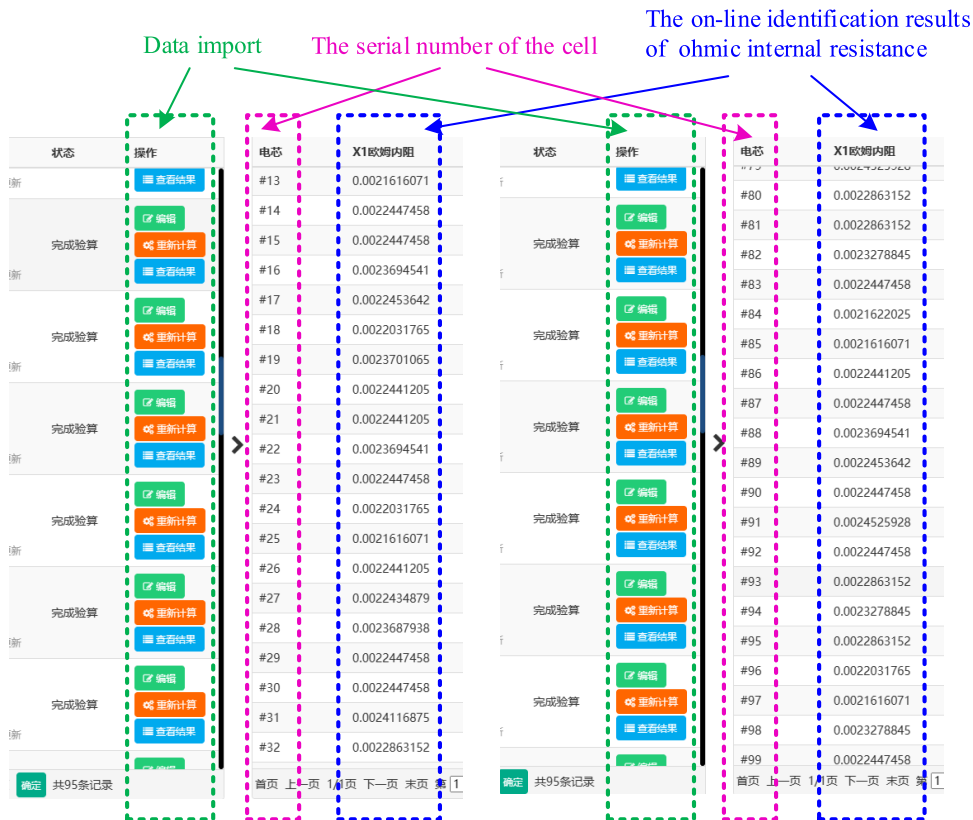**FIGURE 16.** Iinterface of edging computing system.

FIGURE 17. The on-line identification results of ohmic internal resistance.

focuses on internal characteristic parameters such as ohmic internal resistance r_{ohm}, polarization resistance r_p, and polarization capacitance c_p. By the hybrid driving of internal and external characteristic parameters, as shown in Fig. 16, the system achieves effective monitoring of battery health state.

This paper integrates the edge computing platform for battery health management into an energy storage power station in Hunan, China, to demonstrate its practical applicability. Through the real-time monitoring of the voltage and current

of the battery, the online identification of the ohmic internal resistance, polarization resistance and polarization capacitance can be realized.

Taking the battery ohmic internal resistance r_{ohm} as an example, the on-line identification is realized through the operational data, as shown in the following figure.

As can be seen from the figure above, the ohmic internal resistance r_{ohm} identification results of each battery can be viewed, further achieving the hybrid driving of internal and
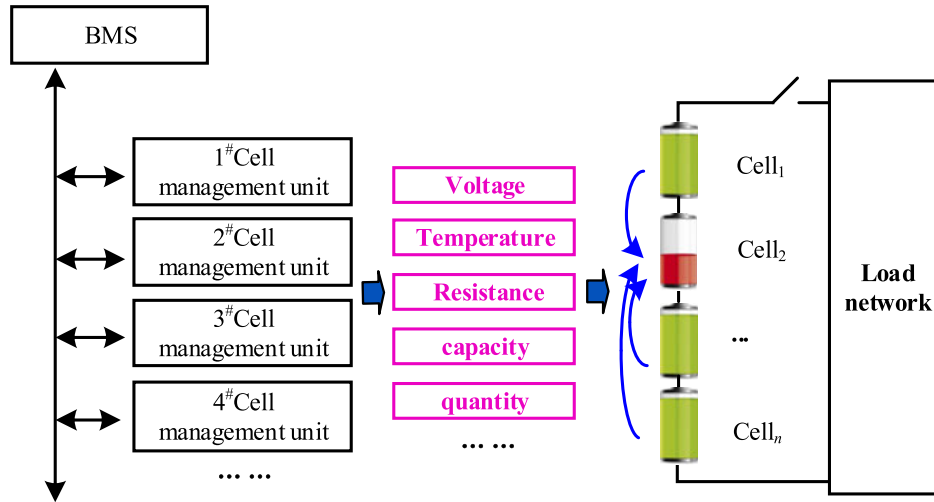
FIGURE 18. Comprehensive evaluation method for consistency.

external characteristic parameters to evaluate battery health state.

Despite its promising applications, edge computing for energy storage batteries still faces challenges and limitations in practical using. For example, it requires high scalability and compatibility to meet the needs of different environments. In addition, due to the large amount of data processing and storage required, the advanced data management and storage technologies are necessary to ensure system stability and reliability. Therefore, further research and development are needed to address these challenges and optimize the performance of edge computing.

IV. SAFETY OPERATION TECHNOLOGIES FOR ENERGY STORAGE STATIONS

On the premise of achieving effective battery state evaluation, the safety operation technologies of energy storage stations are becoming increasingly critical as energy storage equipments are integrated into the power grid. The issues of inconsistency, balancing, circulation, and resonance cannot be ignored.

A. INCONSISTANCY MONITORING OBJECTS

In energy storage power stations, series and parallel batteries connections are required to meet the voltage level and capacity requirements of the storage system. Monitoring the inconsistency among batteries, clusters, and stacks is more crucial than monitoring the health of a single battery. Inconsistencies in the aging degree of energy storage equipment increase the possibility of overcharge, overdischarge, and thermal runaway, which can lead to irreversible safety accidents. As illustrated in Fig. 18, the beginning points of existing research approaches for cell-to-cell variation analysis are not limited to capacity.

(1) From the perspective of terminal voltage, Ref. [90] used the voltage difference based on the pattern distance to detect inconsistencies between batteries. Ref. [91] used the

K-means clustering method with genetic algorithm for the voltage consistency evaluation.

(2) From the perspective of temperatures, Ref. [92] suggested that an uneven temperature can lead to inconsistency in battery packs and impair their performance, and proposed an appropriate working environment temperature. Ref. [93] designed a battery pack with good heat dissipation based on the individual differences in the heat dissipation process of lithium battery packs. Ref. [94] proposed a consistent characterization index for the thermal behavior of battery charging.

(3) From the perspective of impedance, Ref. [95] used multi-points to achieve battery sorting based on the electrochemical impedance spectrum curve.

(4) From the perspective of capacity and quantity, Ref. [96] proposed a two-dimensional vector diagram of "capacity-quantity" to linearize and graph the consistency problem.

(5) From the perspective of multiple objects, Ref. [97] selected capacity, state of charge and resistance as battery pack in consistency parameters. Ref. [27] adopted five indicators of voltage, temperature, internal resistance, capacity, and electricity to calculate the consistency score. Ref. [98] selected the consistency parameters of capacity, internal resistance, and open circuit voltage to analyze the influences on the energy utilization efficiency.

B. ENTROPY FOR INCONSISTENT IDENTIFICATION

A battery pack is composed of batteries that are connected in series and parallel. The battery pack serves as the basic unit for constructing a battery cluster, and battery clusters are in parallel to form a battery stack, as shown in Fig. 19.

During running time, the entire power station stores a large amount of attribute data. Taking a certain energy storage power station in Hunan Province as an example, the main monitored objects include current I, voltage U, temperature T, cumulative charge Q_{char}, cumulative discharge Q_{dis}, state of charge SOC, and state of health SOH. Among them, only
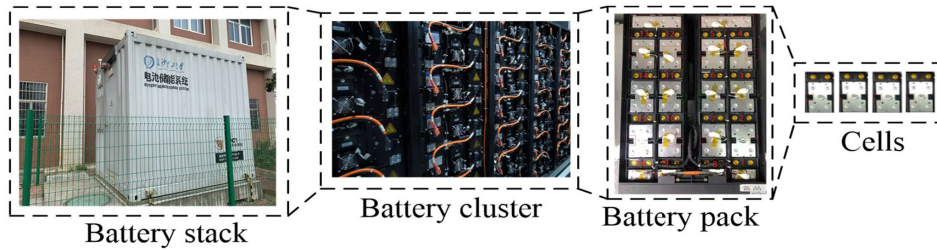
FIGURE 19. Main composition of energy storage power station.

TABLE 6. Types of monitoring data.

Data Composition	Data Name
Measurable Data	Time
	Voltage
	Current
	Temperature
	Average voltage
	Highest voltage
	Lowest voltage
	Average temperature
	Highest temperature
	Lowest temperature
Estimated Data	Cumulative charge of battery cluster
	Cumulative discharge of battery cluster
	SOC of cluster/batteries
	SOH of cluster/batteries

FIGURE 20. Aging of batteries in energy storage power station.

I, U, and T are directly measured attribute data, and the rest are estimated from the above physical quantities, as shown in Tab. 6.

Therefore, this paper proposes preprocessing a large number of attribute data sets, selecting specific operating segment data to form a characteristic data set, and reflecting the overall operation state of the power station through the orderly degree of the characteristic data set. By ensuring the quantity and quality of real-time measurement data, the evaluation accuracy can be guaranteed. This approach provides a more comprehensive and dynamic assessment of the inconsistency, which can help improve the safety and reliability of energy storage systems.

This section focuses on the overall operation state of batteries and uses the sharp voltage drop caused by the ohmic resistance in the initial discharge segment and the highest temperature of batteries within a cluster as an example. The aging degree and inconsistency of batteries are evaluated based on the orderly degree of the sharp voltage drop and the highest temperature data during the discharge process within the cluster, using information entropy [99], [100], [101].

The sampling value of the sharp voltage drop and the highest temperature is normalized as shown in Eq. 12.

$$
\begin{cases}
\lambda_i = \dfrac{\Delta u_{\mathrm{ohm}\_i} - \Delta u_{\mathrm{ohm\_min}}}{\Delta u_{\mathrm{ohm\_max}} - \Delta u_{\mathrm{ohm\_min}}} \\
\mu_t = \dfrac{T_t - T_{\min}}{T_{\max} - T_{\min}}
\end{cases}
\tag{12}
$$

where $\Delta u_{\mathrm{ohm}\_i}$ represents the sharp voltage drop caused by ohmic internal resistance of i-th battery; $\Delta u_{\mathrm{ohm\_min}}$ represents the minimum sharp voltage drop of the batteries; $\Delta u_{\mathrm{ohm\_max}}$ represents the maximum sharp voltage drop of

the batteries; T_t represents the maximum temperature of the batteries in the cluster at the t-th moment; $T_{\max}$ represents the maximum temperature of the batteries; $T_{\min}$ represents the minimum temperature of the batteries.

At the same time, $\lambda = \{\lambda_1, \lambda_2, \ldots, \lambda_N\}$, $\mu = \{\mu_1, \mu_2, \ldots, \mu_M\}$, N is the total number of batteries, and M is the total number of time periods. By counting the number of occurrences $\lambda = \{\lambda_1, \lambda_2, \ldots, \lambda_N\}$ and $\mu = \{\mu_1, \mu_2, \ldots, \mu_M\}$ in different interval ranges, the occurrence probabilities of both can be determined in different intervals, and then the entropy value Δu_{ohm} and T_t can be calculated.

Set a list of equal deviation constants $[a_0, a_1, \ldots, a_{n-1}, a_n)$ and the occurrence frequency of the ratio λ in different interval ranges $[a_0, a_1), [a_1, a_2), \ldots, [a_{n-1}, a_n)$ is counted as $n_{\lambda\_1}, n_{\lambda\_2}, \ldots, n_{\lambda\_k}$, and the occurrence probabilities of the ratio $\lambda = \{\lambda_1, \lambda_2, \ldots, \lambda_N\}$ in different intervals are obtained.

$$
\begin{cases}
P'(1) = \dfrac{n_{\lambda\_1}}{N} \\
P'(2) = \dfrac{n_{\lambda\_2}}{N} \\
\ldots \\
P'(k) = \dfrac{n_{\lambda\_k}}{N}
\end{cases}
\tag{13}
$$

And set a another list of equal deviation constants $[b_0, b_1, \ldots, b_{n-1}, b_n]$ and the occurrence frequency of the ratio μ in different interval ranges $[b_1, b_2), [b_2, b_3), \ldots, [b_{n-1}, b_n)$ is counted as $n_{\mu\_1}, n_{\mu\_2}, \ldots, n_{\mu\_k}$, and the occurrence probabilities of the ratio $\{\mu_1, \mu_2, \ldots, \mu_M\}$ in different intervals are

FIGURE 21. Energy storage system platform and interface of measurment system.

obtained.

$$
\begin{cases}
P''(1) = \dfrac{n_{\mu\_1}}{N} \\
P''(2) = \dfrac{n_{\mu\_2}}{N} \\
\dots \\
P''(l) = \dfrac{n_{\mu\_l}}{N}
\end{cases}
\tag{14}
$$

Based on the occurrence probabilities of the ratio $\{\lambda_1, \lambda_2, \dots, \lambda_N\}$ and $\{\mu_1, \mu_2, \dots, \mu_M\}$ in different intervals, the entropy values of Δu_{ohm} and T_t during the discharge process can be obtained. The calculation formula is as follows:

$$
\begin{cases}
H_{\Delta u} = -\sum_{k=1}^{p} P'(k)\ln P'(k) \\
H_T = -\sum_{l=1}^{q} P''(l)\ln P''(l)
\end{cases}
\tag{15}
$$

where p and q is the number of intervals in different ranges for λ and μ.

If a battery in an energy storage power plant is aging normally, the voltage drop Δu_{ohm} and temperature T_t will gradually increase, and the distribution of λ and μ will exhibit a diffusion trend. However, if a battery is abnormally aged, the maximum voltage drop $\Delta u_{\text{ohm\_max}}$ and maximum temperature $T_{\max}$ will increase, the distribution of λ and μ will become more centralized, as shown in Fig. 20. Different aging conditions will alter the orderliness of the health factor, leading to changes in the information entropy of the data.

To validate the practicality of the suggested method, actual engineering applications were conducted based on a 100kW/200kWh energy storage system platform, as illustrated in Fig. 21. The energy storage system operates under peak shaving and valley filling conditions. The entropy values $H_{\Delta u}$ and H_T were calculated using measured data from the No. 1 cluster of the energy storage system for a random 4-day period.

An arithmetic constant sequence is set as [0, 0.1, …, 0.8, 0.9, 1]. The distribution of the ratio λ is statistically analyzed,
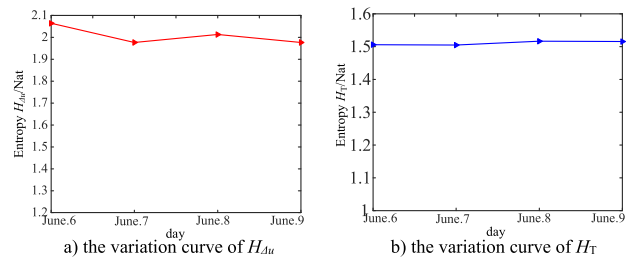

FIGURE 22. Entropy change curve of $H_{\Delta u}$ and H_T.

TABLE 7. Entropy value $H_{\Delta u}$ of characteristic data.

Range	June 6	June 7	June 8	June 9
[0,0.1]	0.0650	0.1324	0.0950	0.1324
[0.1,0.2]	0.1207	0.1909	0.1083	0.1909
[0.2,0.3]	0.2146	0.2944	0.2808	0.2944
[0.3,0.4]	0.2289	0.3238	0.2219	0.3268
[0.4,0.5]	0.2808	0.3268	0.2708	0.3238
[0.5,0.6]	0.3445	0.3066	0.3445	0.3066
[0.6,0.7]	0.2356	0.2146	0.2146	0.2146
[0.7,0.8]	0.3027	0.0950	0.3173	0.0950
[0.8,0.9]	0.1909	0.0650	0.0950	0.0650
[0.9,1]	0.0807	0.0274	0.0650	0.0274
$H_{\Delta u}$	2.0644	1.9769	2.0132	1.9769
SOH	97.4%			

TABLE 8. Entropy value H_T of characteristic data.

Range	June 6	June 7	June 8	June 9
[0,0.2]	0.2922	0.2595	0.2740	0.2804
[0.2,0.4]	0.2714	0.2739	0.2900	0.2859
[0.4,0.6]	0.2581	0.2696	0.2653	0.2666
[0.6,0.8]	0.3171	0.3342	0.3196	0.3153
[0.8,1]	0.3673	0.3679	0.3677	0.3676
H_T	1.5061	1.5051	1.5166	1.5158
SOH	97.4%			

and the entropy values $H_{\Delta u}$ are calculated, as shown in the Tab. 7.

Similarly, an another arithmetic constant sequence is set as [0, 0.2, …, 0.8, 1], and the distribution of ratio μ is statistically analyzed. The entropy values H_T are calculated, as shown in the Tab. 8.

Based on the entropy values in Tab. 7 and Tab. 8, the variation curve is drawn, as shown in Fig. 22.

a) Graph model of a single battery to a pack balancing topology

b) Graph model of a pack to a single battery balancing topology

c) Graph model of a adjacent battery to a adjacent battery balancing topology

d) Graph model of a arbitrary battery to a arbitrary battery balancing topology
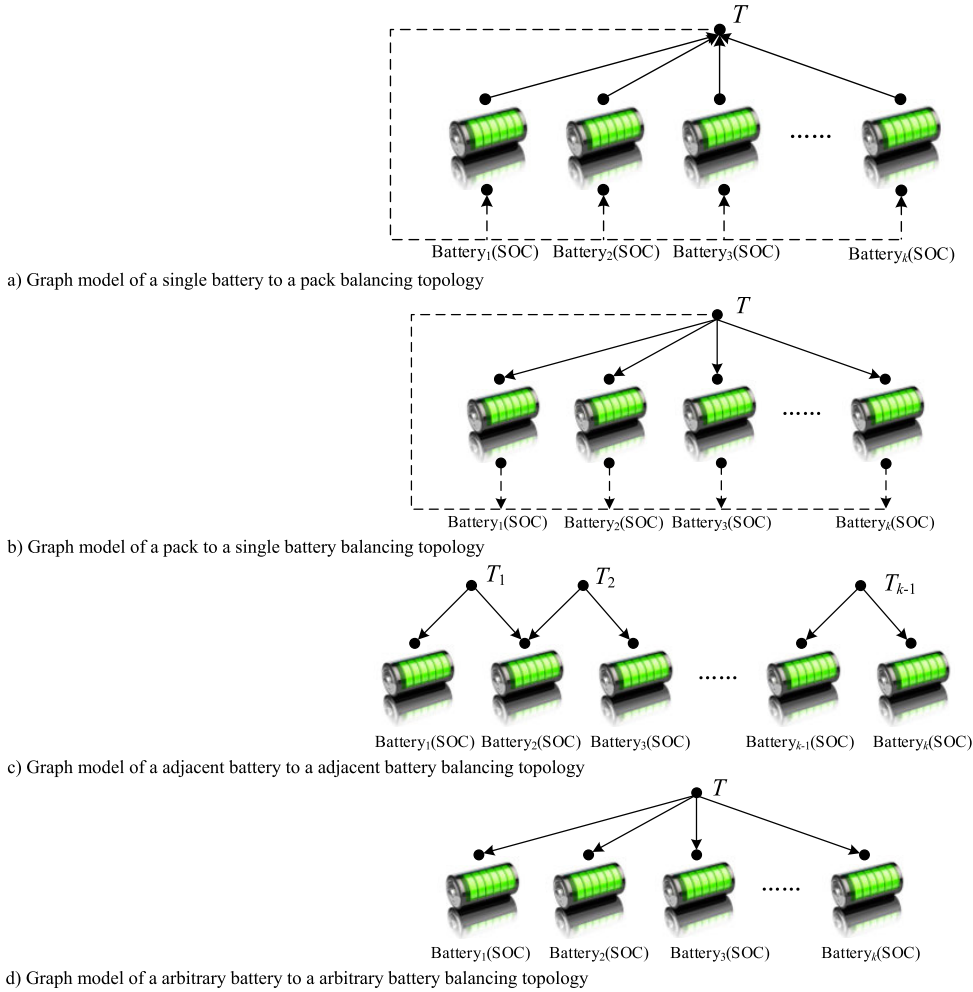
FIGURE 23. Graph model of different balancing topologies.

Tab. 7 and Fig. 22(a) show that the entropy value $H_{\Delta u}$ of the voltage drop amplitude Δu_{ohm} caused by the batteries' ohmic internal resistance in the initial discharge segment remains stable within the range of 1.9 to 2.1. Tab. 8 and Fig. 22(b) show that the entropy value H_T of the highest temperature T_t of the cluster's batteries remains stable between 1.50 and 1.52. The above characteristic data shows a reasonably high degree of order, indicating that the battery cluster is in good condition.

At the same time, the SOH monitoring results of energy storage equipment for a random four-day period are 97.4%. The conclusion of the information entropy evaluation is consistent with the monitoring data, confirming the method's effectiveness and having practical engineering application value.

Therefore, the entropy value of the characteristic data set for batteries is strongly correlated with the health state of the energy storage station. If real-time monitoring of the characteristic data set for batteries within the cluster is ensured, the entropy value can serve as an effective evaluation metric for the inconsistency, preventing serious accidents.

C. BALANCING TOPOLOGY

The balanced topology structure should possess bidirectional properties, including energy spanning transmission, the absence of balancing overlap issues, effective balancing performance, ease of expansion, and simple circuit construction. Assuming that the efficiency of the different equalizers is σ, remaining constant.

The main topological structure can be classified into four categories [102], [103]:

(1) A single battery to a pack: when the voltage of a single battery is high, the excess energy is first transferred to the auxiliary equipment T, and then to the entire battery pack. The energy transfer path is $B_i \rightarrow T \rightarrow \{B_1, B_2, \ldots \rightarrow B_n\}$, as shown in Fig. 23-a. Assuming that the excess energy of a single battery is P and the number of batteries is k, the excess energy is distributed across all batteries, and the average balanced efficiency is illustrated in Tab. 9.

(2) A pack to a single battery: when the voltage or energy of a battery is insufficient, the entire battery pack charges the battery via auxiliary equipment T. And the energy transfer path is $\{B_1, B_2, \ldots \rightarrow B_n\} \rightarrow T \rightarrow B_i$, as shown in Fig. 23-b; the average balanced efficiency is illustrated in Tab. 9.

TABLE 9. The average balanced efficiency of different Graph models.

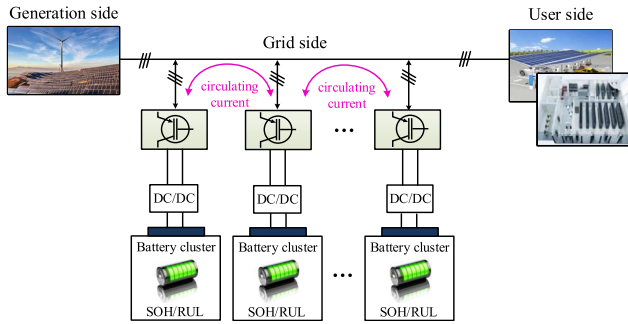| The topological structure	Average balanced efficiency
A single battery to a pack	$\dfrac{k-1}{k}\sigma$
A pack to a single battery	$\dfrac{k-1}{k}\sigma$
A adjacent battery to a adjacent battery	$\dfrac{2n\sigma(1-\sigma)-2\sigma(1-\sigma^n)}{n(n-1)(1-\sigma)^2}$
A arbitrary battery to a arbitrary battery	σ^2

FIGURE 24. Grid model of energy storage system.

(3) A adjacent battery to a adjacent battery: when there is an energy difference between two neighboring batteries and an auxiliary device T_i is located between them, energy is transferred from the higher one to the lower one. The shortest path is $B_i \rightarrow T_i \rightarrow B_{i+1}$, and the longest path is $B_1 \rightarrow T_1 \rightarrow B_2 \ldots B_{n-1} \rightarrow T_{n-1} \rightarrow B_n$, as shown in Fig. 23-c;. The average balanced efficiency is illustrated in Tab. 9.

(4) A arbitrary battery to a arbitrary battery: the battery with the highest voltage or energy is transferred to the battery with the lowest voltage or energy, and the auxiliary device T alternates between batteries that require energy exchange. The energy transfer path is $B_i \rightarrow T \rightarrow B_j$, as shown in Fig. 23-d. The average balanced efficiency is illustrated in Tab. 9.

D. CIRCULATION AND RESONANCE

In large-scale energy storage systems, the number of parallel battery clusters increases the current of the battery stack, resulting in stricter requirements for the consistency of the battery clusters' operation, as shown in Fig. 24.

Manufacturing processes, charging or discharging methods, and environmental factors can cause inconsistency in the long-term use of lithium-ion batteries, resulting in some battery clusters being in a deep state of charge and discharge for a long time while others have little output. These inconsistencies not only affect the available capacity of energy storage stations but also generate inter-cluster circulation, which can cause further degradation of battery health. Therefore, it is crucial to ensure the consistency of battery clusters' operation and prevent inter-cluster circulation to maintain the health and longevity of energy storage systems.
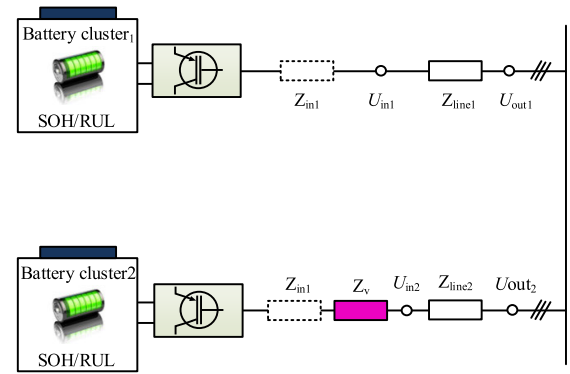

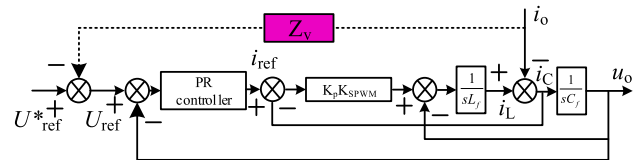**FIGURE 25. Parallel structure of battery clusters with virtual impedance added.**

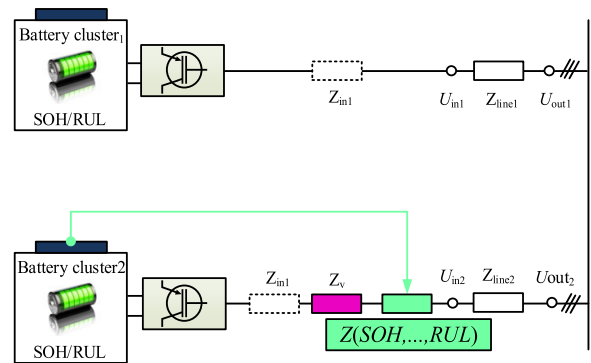**FIGURE 26. Control block of inverter introducing virtual impedance.**

FIGURE 27. Parallel structure of battery clusters with virtual impedance added.

To achieve power decoupling and circulating current elimination, virtual impedance values are rationally designed to match the equivalent line impedance of parallel branches. The parallel structure of multi-converters implementing virtual impedance is shown in Fig. 25. This design can effectively eliminate the inter-cluster circulation caused by inconsistency in battery clusters' operation and ensure the consistency of energy storage systems, thereby improving the overall performance and longevity of the system [104], [105].

In Fig. 25, Z_v is the virtual impedance value introduced into the converter parallel system, including the virtual resistance value R_v and the virtual reactance value X_v; Z_{lines} is the equivalent line impedance value of the converter parallel system.

Therefore, the converter control block diagram introducing virtual impedance is shown in Fig. 28.

As shown in the above figure, the control strategy mainly adjusts by introducing virtual impedance to keep the output voltage and current of each inverter consistent.

However, this control strategy defaults to considering aging degrees and ignores aging differences between battery clusters. As a result, the control method should consider the
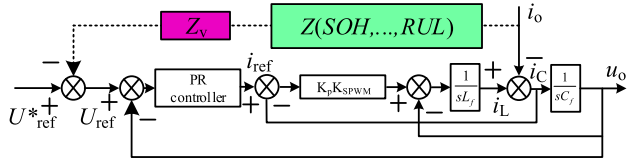
FIGURE 28. Control block of inverter considering inconsistent aging degree of battery clusters.
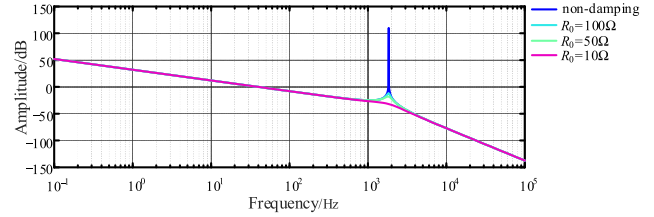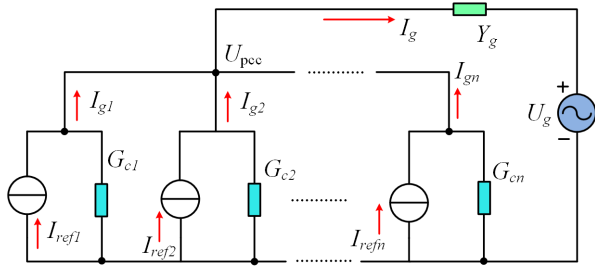

FIGURE 29. Structure of multi-converters parallel system based on current source equivalence.

FIGURE 30. Control block diagram under parallel resistance of filtering capacitor.
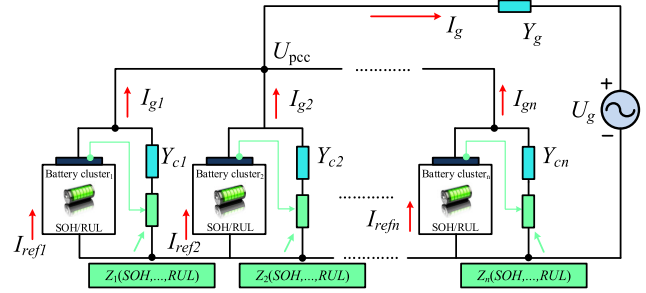

FIGURE 31. The bode diagram.

FIGURE 32. Structure of multi-conmultis parallel system considering inconsistent aging degree of battery clusters.

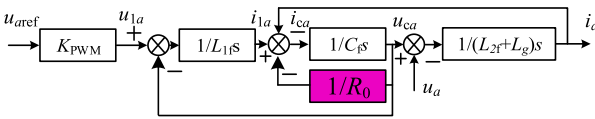**FIGURE 33.** Control block diagram of filtering capacitors considering aging degree of battery clusters.
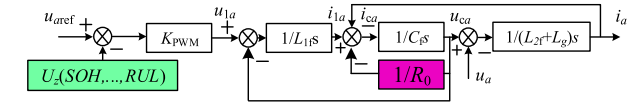

FIGURE 34. The schematic diagram for intelligent inspection robot.

SOH and RUL of the energy storage equipment, as seen in Fig. 27. By incorporating these factors into the control strategy, it is possible to achieve more precise and effective control of energy storage systems and ensure the longevity and optimal performance of the system.

The control strategy is shown in the following figure.

The resonance difficulties occur not only in each inverter's LCL filter, but also in interactions between the phase-locked loop and the control loop, between the converter and the converter, and between the converter and the power grid, resulting in system instability.

In resonance analysis, grid-connected converter systems frequently use current closed-loop control, which can be equal to a Norton equivalent circuit of current source shunt admittance, as shown below. This approach can effectively suppress the oscillations and improve the stability of the system.

As the number of grid-connected converters increases, resulting in equivalent impedance at the PCC and harmonic amplification of the grid voltage, the possibility of resonance in multi-converter parallel systems increases, affecting output power quality, dynamic response, and system stability [106], [107]. Simultaneously, the resonance will have the opposite effect on the energy storage equipment.

The passive damping control employs series and parallel resistors to suppress the resonant peaks. For example, the filter capacitor and resistor are connected in paralle to suppress the resonant peaks, the control block diagram is shown in Fig. 30. This approach can effectively reduce the oscillations in the system and improve its stability.

The transfer function from grid-side current to inverter output voltage is, as in (16), shown at the bottom of the next page.

The Bode diagram of $G_{LCL}(s)$ is shown in Fig. 33.

As shown in Fig. 31, a suitable resistor connected in parallel with a filter capacitor successfully suppresses resonance spikes while maintaining filtering performance in the low and high frequency ranges.

However, the degree of aging of battery clusters varies, resulting in changes in the impedance of each loop. The above technique assumes a consistent degree of aging between battery clusters, ignoring their aging variances. As a result, the SOH and RUL of energy storage equipment should be taken into account. In Fig. 32, it depicts the topology of a multi-converter parallel system, taking the aging degree of battery clusters into account.

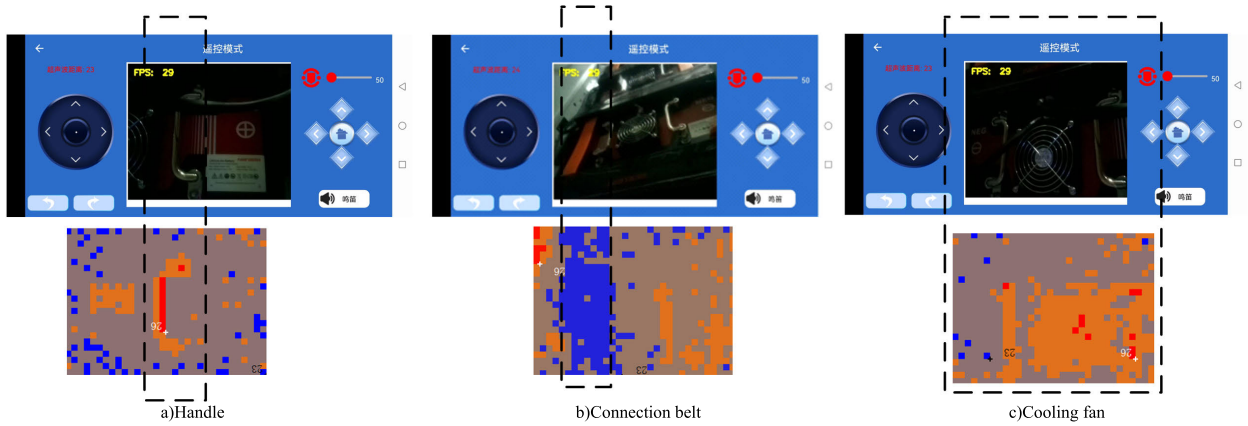The control strategy is shown in the following figure.

FIGURE 35. The thermal imaging results for intelligent inspection robot.

E. INTELLIGENT INSPECTION ROBOT

The information will be transmitted to the EMS for correct judgment and safety control after the inconsistency, circulation, and resonance of energy storage equipment are effectively monitored. As a result, we focus on developing an intelligent inspection robot for energy storage stations, as shown in Fig. 34, which includes a mobile system, a high-definition camera, an infrared temperature module (MLX90640-D110), and a message acceptance module (TCP/IP protocol), allowing for real-time data interaction with the EMS as well as rapid inspection and diagnosis of inconsistency, circulation, and resonance issues.

Simultaneously, by setting a predetermined path, the inspection robot uses infrared thermography for non-contact temperature measurements. The acquired temperature matrix is then converted into a color cloud map, which displays the highest and lowest temperatures inside the matrix.

Based on a 100kW/200kWh energy storage system architecture, this article employs an intelligent inspection robot to perform thermal scanning of battery packs. The intelligent inspection robot inspects the target battery pack on a planned basis using the EMS's evaluation results and real-time data interaction. The PC workstation's program interface not only records video images of the handle, connecting belt, and cooling fan, but it also precisely shows their temperature cloud maps, as illustrated in Fig. 35, allowing for rapid examination and real-time diagnosis.

To summarize, the intelligent control mobile robot conducts targeted inspections and periodic patrols, and it can be integrated with cloud platforms to accurately assess the overall safety state of batteries.

V. CONCLUSION

The architecture of the power system is about to shift from "source-grid-load" to "source-net-load-stock". This paper discusses and deals with topics such as effective battery condition assessment, edge computing platform, inconsistency analysis, and multi-target control of energy storage equipment.

(1) Battery state evaluation has widely used various methods, such as equivalent circuit models and data-driven methods, as well as diverse health factors, such as voltage change rate, current change rate, and temperature change rate in the CC/CV charging process, to ensure battery efficiency, reliability, and safety.

(2) In review of battery state evaluation based on fragmented data, this paper proposes two methods from the perspectives of the empirical fitting model and the machine learning model, as well as our views on state prediction using fragmented data. The proposed method in this paper was validated using NASA lithium-ion battery aging data, with MAE values of 0.0249 A·h and 0.0154 A·h, maintaining a low level. And the applicability of state prediction for other types of batteries will be further investigated.

(3) Based on the existing edge computing platform, only the battery external characteristics (current, voltage, and temperature) are monitored. This paper considers the construction of edge computing platforms should also be based on effective monitoring of the internal characteristics of batteries, such as ohmic internal resistance r_{ohm}, polarization resistance r_p, and polarization capacitance c_p. Based on this, this article constructs an edge platform that achieves effective monitoring of battery health state by combining both internal and external characteristics. This platform achieves a more comprehensive assessment of the battery health state through the hybrid driving of internal and external characteristic parameters and helps identify potential safety issues.

(4) The concept of information entropy can be transplanted to the specific operation segment data of the energy storage plant for inconsistency analysis. Based on a 100kW/200kWh energy storage system platform and selecting operational data for four days randomly, the entropy value $H_{\Delta u}$ of the voltage

$$G_{LCL}(s) = \frac{R_0}{L_{1f}\left(L_{2f} + L_g\right) C_f R_0 s^3 + L_{1f}\left(L_{2f} + L_g\right) s^2 + R_0\left(L_{1f} + L_{2f} + L_g\right) s} \quad (16)$$

drop amplitude Δu_{ohm} of the batteries remains stable within the range of 1.9 to 2.1. The entropy value H_T of the highest temperature T_t of the batteries remains stable within the range of 1.50 to 1.52. This indicates that if the energy storage power station is in good health, the entropy values of the characteristic data will remain stable within a certain range.

(5) The control strategies proposed in this paper prioritize the SOH, RUL, and other safety indicators for each battery cluster while addressing the issues of energy storage system circulation and resonance. This is aimed at further optimizing the output power range of the battery clusters.

(6) To monitor the safety of energy storage power plants, we created an intelligent inspection robot equipped with a mobile system, a high-definition camera, an infrared temperature module, and a message acceptance module. The robot can interact with the EMS platform, allowing for rapid inspection and real-time diagnosis of inconsistency, circulation, and resonance.

The paper offers new concepts and theoretical support for battery state evaluation and energy storage power station safety operations. These findings are crucial for the development of new power systems that take into account the safety, efficiency, and longevity of batteries, contributing to the advancement of energy storage technologies and helping promote the widespread adoption of renewable energy.

When the size and configuration of energy storage power plants change, adjustments will be made to the proposed solutions for safety operation technologies, such as data storage capacity and transfer functions for control strategies. However, the main focus of the solutions, such as inconsistency, balancing, circulation, and resonance, will not change. As a result, the views suggested in this paper are widely applicable.

REFERENCES

[1] R. Xiong, L. Li, and J. Tian, "Towards a smarter battery management system: A critical review on battery state of health monitoring methods," *J. Power Sources*, vol. 405, pp. 18–29, Nov. 2018.

[2] E. Kim, M. Kim, J. Kim, J. Kim, J.-H. Park, K.-T. Kim, J.-H. Park, T. Kim, and K. Min, "Data-driven methods for predicting the state of health, state of charge, and remaining useful life of Li-ion batteries: A comprehensive review," *Int. J. Precis. Eng. Manuf.*, vol. 24, no. 7, pp. 1281–1304, Jul. 2023.

[3] Z. Yi, Z. Chen, K. Yin, L. Wang, and K. Wang, "Sensing as the key to the safety and sustainability of new energy storage devices," *Protection Control Modern Power Syst.*, vol. 8, no. 1, pp. 431–452, Dec. 2023.

[4] M. Elmahallawy, T. Elfouly, A. Alouani, and A. M. Massoud, "A comprehensive review of lithium-ion batteries modeling, and state of health and remaining useful lifetime prediction," *IEEE Access*, vol. 10, pp. 119040–119070, 2022.

[5] H. Tian, P. Qin, K. Li, and Z. Zhao, "A review of the state of health for lithium-ion batteries: Research status and suggestions," *J. Cleaner Prod.*, vol. 261, Jul. 2020, Art. no. 120813.

[6] M. S. Hossain Lipu, S. Ansari, M. S. Miah, S. T. Meraj, K. Hasan, A. S. M. Shihavuddin, M. A. Hannan, K. M. Muttaqi, and A. Hussain, "Deep learning enabled state of charge, state of health and remaining useful life estimation for smart battery management system: Methods, implementations, issues and prospects," *J. Energy Storage*, vol. 55, Nov. 2022, Art. no. 105752.

[7] M. Abedi Varnosfaderani and D. Strickland, "A comparison of online electrochemical spectroscopy impedance estimation of batteries," *IEEE Access*, vol. 6, pp. 23668–23677, 2018.

[8] B. Jiang, J. Zhu, X. Wang, X. Wei, W. Shang, and H. Dai, "A comparative study of different features extracted from electrochemical impedance spectroscopy in state of health estimation for lithium-ion batteries," *Appl. Energy*, vol. 322, Sep. 2022, Art. no. 119502.

[9] D. Andre, M. Meiler, K. Steiner, H. Walz, T. Soczka-Guth, and D. U. Sauer, "Characterization of high-power lithium-ion batteries by electrochemical impedance spectroscopy. II: Modelling," *J. Power Sources*, vol. 196, no. 12, pp. 5349–5356, Jun. 2011.

[10] K. Mc Carthy, H. Gullapalli, K. M. Ryan, and T. Kennedy, "Review—Use of impedance spectroscopy for the estimation of Li-ion battery state of charge, state of health and internal temperature," *J. Electrochem. Soc.*, vol. 168, no. 8, Aug. 2021, Art. no. 080517.

[11] X. Liu, K. Li, J. Wu, Y. He, and X. Liu, "An extended Kalman filter based data-driven method for state of charge estimation of Li-ion batteries," *J. Energy Storage*, vol. 40, Aug. 2021, Art. no. 102655.

[12] C. Lin, H. Mu, R. Xiong, and W. Shen, "A novel multi-model probability battery state of charge estimation approach for electric vehicles using H-infinity algorithm," *Appl. Energy*, vol. 166, pp. 76–83, Mar. 2016.

[13] J. Du, Z. Liu, Y. Wang, and C. Wen, "An adaptive sliding mode observer for lithium-ion battery state of charge and state of health estimation in electric vehicles," *Control Eng. Pract.*, vol. 54, pp. 81–90, Sep. 2016.

[14] S. Amir, M. Gulzar, M. O. Tarar, I. H. Naqvi, N. A. Zaffar, and M. G. Pecht, "Dynamic equivalent circuit model to estimate state-of-health of lithium-ion batteries," *IEEE Access*, vol. 10, pp. 18279–18288, 2022.

[15] H. He, X. Zhang, R. Xiong, Y. Xu, and H. Guo, "Online model-based estimation of state-of-charge and open-circuit voltage of lithium-ion batteries in electric vehicles," *Energy*, vol. 39, no. 1, pp. 310–318, Mar. 2012.

[16] X. He, B. Sun, W. Zhang, X. Fan, X. Su, and H. Ruan, "Multi-time scale variable-order equivalent circuit model for virtual battery considering initial polarization condition of lithium-ion battery," *Energy*, vol. 244, Apr. 2022, Art. no. 123084.

[17] T. Oji, Y. Zhou, S. Ci, F. Kang, X. Chen, and X. Liu, "Data-driven methods for battery SOH estimation: Survey and a critical analysis," *IEEE Access*, vol. 9, pp. 126903–126916, 2021.

[18] Y. Li, K. Liu, A. M. Foley, A. Zülke, M. Berecibar, E. Nanini-Maury, J. Van Mierlo, and H. E. Hoster, "Data-driven health estimation and lifetime prediction of lithium-ion batteries: A review," *Renew. Sustain. Energy Rev.*, vol. 113, Oct. 2019, Art. no. 109254.

[19] A. Nuhic, T. Terzimehic, T. Soczka-Guth, M. Buchholz, and K. Dietmayer, "Health diagnosis and remaining useful life prognostics of lithium-ion batteries using data-driven methods," *J. Power Sources*, vol. 239, pp. 680–688, Oct. 2013.

[20] H. Feng and X. Zhang, "State of health estimation and remaining using life prediction of lithium-ion batteries based on new health indicators," (in Chinese), *J. Nanjing Univ.*, vol. 57, no. 4, pp. 660–670, 2021.

[21] J. Xu, Y. Ni, and C. Zhu, "Remaining useful life prediction for lithium-ion batteries based on improved support vector regression," *Trans. China Electrotech. Soc.*, vol. 36, no. 17, pp. 3693–3704, 2021.

[22] D. Liu, H. Wang, Y. Peng, W. Xie, and H. Liao, "Satellite lithium-ion battery remaining cycle life prediction with novel indirect health indicator extraction," *Energies*, vol. 6, no. 8, pp. 3654–3668, Jul. 2013.

[23] C. Weng, X. Feng, J. Sun, and H. Peng, "State-of-health monitoring of lithium-ion battery modules and packs via incremental capacity peak tracking," *Appl. Energy*, vol. 180, pp. 360–368, Oct. 2016.

[24] X. Bian, Z. Wei, W. Li, J. Pou, D. U. Sauer, and L. Liu, "State-of-health estimation of lithium-ion batteries by fusing an open-circuit-voltage model and incremental capacity analysis," *IEEE Trans. Power Electron.*, vol. 37, no. 2, pp. 2226–2236, Aug. 2022.

[25] B. Ospina Agudelo, W. Zamboni, and E. Monmasson, "Application domain extension of incremental capacity-based battery SoH indicators," *Energy*, vol. 234, Nov. 2021, Art. no. 121224.

[26] J. Tian, Y. Fan, T. Pan, X. Zhang, J. Yin, and Q. Zhang, "A critical review on inconsistency mechanism, evaluation methods and improvement measures for lithium-ion battery energy storage systems," *Renew. Sustain. Energy Rev.*, vol. 189, Jan. 2024, Art. no. 113978.

[27] Y. Lu, K. Li, X. Han, X. Feng, Z. Chu, L. Lu, P. Huang, Z. Zhang, Y. Zhang, F. Yin, X. Wang, F. Dai, M. Ouyang, and Y. Zheng, "A method of cell-to-cell variation evaluation for battery packs in electric vehicles with charging cloud data," *eTransportation*, vol. 6, Nov. 2020, Art. no. 100077.

[28] J. Wang and L. Ruan, "Cell-to-cell inconsistency analysis and structure optimization for a liquid-cooled cylindrical battery module," *Appl. Thermal Eng.*, vol. 224, Apr. 2023, Art. no. 120021.

[29] J. Tian, X. Liu, C. Chen, G. Xiao, Y. Wang, Y. Kang, and P. Wang, "Feature fusion-based inconsistency evaluation for battery pack: Improved Gaussian mixture model," *IEEE Trans. Intell. Transp. Syst.*, vol. 24, no. 1, pp. 446–458, Jan. 2023.

[30] P. Dong, Z. Liu, P. Wu, Z. Li, Z. Wang, and J. Zhang, "Reliable and early warning of lithium-ion battery thermal runaway based on electrochemical impedance spectrum," *J. Electrochem. Soc.*, vol. 168, no. 9, Sep. 2021, Art. no. 090529.

[31] M. Messing, T. Shoa, and S. Habibi, "Electrochemical impedance spectroscopy with practical rest-times for battery management applications," *IEEE Access*, vol. 9, pp. 66989–66998, 2021.

[32] S. Nejad, D. T. Gladwin, and D. A. Stone, "A systematic review of lumped-parameter equivalent circuit models for real-time estimation of lithium-ion battery states," *J. Power Sources*, vol. 316, pp. 183–196, Jun. 2016.

[33] X. Ding, D. Zhang, J. Cheng, B. Wang, and P. C. K. Luk, "An improved Thevenin model of lithium-ion battery with high accuracy for electric vehicles," *Appl. Energy*, vol. 254, Nov. 2019, Art. no. 113615.

[34] Y. Song, Y. Peng, and D. Liu, "Model-based health diagnosis for lithium-ion battery pack in space applications," *IEEE Trans. Ind. Electron.*, vol. 68, no. 12, pp. 12375–12384, Dec. 2021.

[35] W. Zhang, L. Wang, L. Wang, C. Liao, and Y. Zhang, "Joint state-of-charge and state-of-available-power estimation based on the online parameter identification of lithium-ion battery model," *IEEE Trans. Ind. Electron.*, vol. 69, no. 4, pp. 3677–3688, Apr. 2022.

[36] Q. Wang, T. Gao, and X. Li, "SOC estimation of lithium-ion battery based on equivalent circuit model with variable parameters," *Energies*, vol. 15, no. 16, p. 5829, Aug. 2022.

[37] Y. Zhang, Y. Liu, J. Wang, and T. Zhang, "State-of-health estimation for lithium-ion batteries by combining model-based incremental capacity analysis with support vector regression," *Energy*, vol. 239, Jan. 2022, Art. no. 121986.

[38] Q. Li, D. Li, K. Zhao, L. Wang, and K. Wang, "State of health estimation of lithium-ion battery based on improved ant lion optimization and support vector regression," *J. Energy Storage*, vol. 50, Jun. 2022, Art. no. 104215.

[39] J. Tian, R. Xiong, and W. Shen, "State-of-Health estimation based on differential temperature for lithium ion batteries," *IEEE Trans. Power Electron.*, vol. 35, no. 10, pp. 10363–10373, Oct. 2020.

[40] D. Zhou, H. Yin, P. Fu, X. Song, W. Lu, L. Yuan, and Z. Fu, "Prognostics for state of health of lithium-ion batteries based on Gaussian process regression," *Math. Problems Eng.*, vol. 174, Jun. 2018, Art. no. 8358025.

[41] P. Wang, X. Peng, and C. Ze, "State-of-health estimation for lithium-ion batteries using differential thermal voltammetry and Gaussian process regression," *J. Power Electron.*, vol. 22, no. 7, pp. 1165–1175, Jul. 2022.

[42] D. Yang, X. Zhang, R. Pan, Y. Wang, and Z. Chen, "A novel Gaussian process regression model for state-of-health estimation of lithium-ion battery using charging curve," *J. Power Sources*, vol. 384, pp. 387–395, Apr. 2018.

[43] M. El-Dalahmeh, J. Lillystone, M. Al-Greer, and M. El-Dalahmeh, "State of health estimation of lithium-ion batteries based on data-driven techniques," in *Proc. 56th Int. Universities Power Eng. Conf. (UPEC)*, Aug. 2021, pp. 1–6.

[44] L. Zhang, J. Zhang, T. Gao, L. Lyu, L. Wang, W. Shi, L. Jiang, and G. Cai, "Improved LSTM based state of health estimation using random segments of the charging curves for lithium-ion batteries," *J. Energy Storage*, vol. 74, Dec. 2023, Art. no. 109370.

[45] M.-S. Park, J.-K. Lee, and B.-W. Kim, "SOH estimation of Li-ion battery using discrete wavelet transform and long short-term memory neural network," *Appl. Sci.*, vol. 12, no. 8, p. 3996, Apr. 2022.

[46] Y. Ma, C. Shan, J. Gao, and H. Chen, "A novel method for state of health estimation of lithium-ion batteries based on improved LSTM and health indicators extraction," *Energy*, vol. 251, Jul. 2022, Art. no. 123973.

[47] Y. Fu, J. Xu, M. Shi, and X. Mei, "A fast impedance calculation-based battery state-of-health estimation method," *IEEE Trans. Ind. Electron.*, vol. 69, no. 7, pp. 7019–7028, Jul. 2022.

[48] M. Jiao, Y. Yang, D. Wang, and P. Gong, "The conjugate gradient optimized regularized extreme learning machine for estimating state of charge," *Ionics*, vol. 27, no. 11, pp. 4839–4848, Nov. 2021.

[49] W. Duan, S. Song, F. Xiao, Y. Chen, S. Peng, and C. Song, "Battery SOH estimation and RUL prediction framework based on variable forgetting factor online sequential extreme learning machine and particle filter," *J. Energy Storage*, vol. 65, Aug. 2023, Art. no. 107322.

[50] J. Wen, X. Chen, X. Li, and Y. Li, "SOH prediction of lithium battery based on IC curve feature and BP neural network," *Energy*, vol. 261, Dec. 2022, Art. no. 125234.

[51] R. Xiong, S. Wang, C. Yu, C. Fernandez, W. Xiao, and J. Jia, "A novel nonlinear decreasing step-bacterial foraging optimization algorithm and simulated annealing-back propagation model for long-term battery state of health estimation," *J. Energy Storage*, vol. 59, Mar. 2023, Art. no. 106484.

[52] Z. Fan, X. Zi-xuan, and W. Ming-hu, "State of health estimation for Li-ion battery using characteristic voltage intervals and genetic algorithm optimized back propagation neural network," *J. Energy Storage*, vol. 57, Jan. 2023, Art. no. 106277.

[53] A. Guha and A. Patra, "State of health estimation of lithium-ion batteries using capacity fade and internal resistance growth models," *IEEE Trans. Transport. Electrific.*, vol. 4, no. 1, pp. 135–146, Mar. 2018.

[54] X. Sun, K. Zhong, and M. Han, "A hybrid prognostic strategy with unscented particle filter and optimized multiple kernel relevance vector machine for lithium-ion battery," *Measurement*, vol. 170, Jan. 2021, Art. no. 108679.

[55] X. Li, C. Yuan, and Z. Wang, "State of health estimation for Li-ion battery via partial incremental capacity analysis based on support vector regression," *Energy*, vol. 203, Jul. 2021, Art. no. 117852.

[56] B. Gou, Y. Xu, and X. Feng, "State-of-health estimation and remaining-useful-life prediction for lithium-ion battery using a hybrid data-driven method," *IEEE Trans. Veh. Technol.*, vol. 69, no. 10, pp. 10854–10867, Oct. 2020.

[57] Q. Zhang, X. Li, C. Zhou, Y. Zou, Z. Du, M. Sun, Y. Ouyang, D. Yang, and Q. Liao, "State-of-health estimation of batteries in an energy storage system based on the actual operating parameters," *J. Power Sources*, vol. 506, Sep. 2021, Art. no. 230162.

[58] H. Sun, D. Yang, J. Du, P. Li, and K. Wang, "Prediction of Li-ion battery state of health based on data-driven algorithm," *Energy Rep.*, vol. 8, pp. 442–449, Nov. 2022.

[59] Y. Li, P. Huang, L. T. Gao, C. Zhao, and Z.-S. Guo, "Data-driven state of health estimation for lithium-ion batteries based on universal feature selection," *J. Electrochem. Soc.*, vol. 170, no. 4, Apr. 2023, Art. no. 040507.

[60] Z. Chen, Q. Xue, R. Xiao, Y. Liu, and J. Shen, "State of health estimation for lithium-ion batteries based on fusion of autoregressive moving average model and Elman neural network," *IEEE Access*, vol. 7, pp. 102662–102678, 2019.

[61] X. Pang, X. Liu, J. Jia, J. Wen, Y. Shi, J. Zeng, and Z. Zhao, "A lithium-ion battery remaining useful life prediction method based on the incremental capacity analysis and Gaussian process regression," *Microelectron. Rel.*, vol. 127, Dec. 2021, Art. no. 114405.

[62] Y. Li, M. Abdel-Monem, R. Gopalakrishnan, M. Berecibar, E. Nanini-Maury, N. Omar, P. van den Bossche, and J. Van Mierlo, "A quick on-line state of health estimation method for Li-ion battery with incremental capacity curves processed by Gaussian filter," *J. Power Sources*, vol. 373, pp. 40–53, Jan. 2018.

[63] E. Schaltz, D.-I. Stroe, K. Nørregaard, L. S. Ingvardsen, and A. Christensen, "Incremental capacity analysis applied on electric vehicles for battery state-of-health estimation," *IEEE Trans. Ind. Appl.*, vol. 57, no. 2, pp. 1810–1817, Mar. 2021.

[64] X. Tang, C. Zou, K. Yao, G. Chen, B. Liu, Z. He, and F. Gao, "A fast estimation algorithm for lithium-ion battery state of health," *J. Power Sources*, vol. 396, pp. 453–458, Aug. 2018.

[65] J. Wu, C. Zhang, and Z. Chen, "An online method for lithium-ion battery remaining useful life estimation using importance sampling and neural networks," *Appl. Energy*, vol. 173, pp. 134–140, Jul. 2016.

[66] Y. Zhou, M. Huang, Y. Chen, and Y. Tao, "A novel health indicator for on-line lithium-ion batteries remaining useful life prediction," *J. Power Sources*, vol. 321, pp. 1–10, Jul. 2016.

[67] J. Zhao, Y. Zhu, B. Zhang, M. Liu, J. Wang, C. Liu, and Y. Zhang, "Method of predicting SOH and RUL of lithium-ion battery based on the combination of LSTM and GPR," *Sustainability*, vol. 14, no. 19, p. 11865, Sep. 2022.

[68] W. Liu and Y. Xu, "Data-driven online health estimation of Li-ion batteries using a novel energy-based health indicator," *IEEE Trans. Energy Convers.*, vol. 35, no. 3, pp. 1715–1718, Sep. 2020.

[69] S. Zhang, S. Wu, G. Cao, and X. Zhang, "Capacity estimation for lithium-ion battery via a novel health indicator extracted from partial constant voltage charging curve," *J. Cleaner Prod.*, vol. 409, Jul. 2023, Art. no. 137220.

[70] R. Wang and H. Feng, "Remaining useful life prediction of lithium-ion battery using a novel health indicator," *Qual. Rel. Eng. Int.*, vol. 37, no. 3, pp. 1232–1243, Apr. 2021.

[71] X. Hou, X. Guo, Y. Yuan, K. Zhao, L. Tong, C. Yuan, and L. Teng, "The state of health prediction of Li-ion batteries based on an improved extreme learning machine," *J. Energy Storage*, vol. 70, Oct. 2023, Art. no. 108044.

[72] J. Chen, Y. Hu, Q. Zhu, H. Rashid, and H. Li, "A novel battery health indicator and PSO-LSSVR for LiFePO$_4$ battery SOH estimation during constant current charging," *Energy*, vol. 282, Nov. 2023, Art. no. 128782.

[73] Q. Zhao, X. Qin, H. Zhao, and W. Feng, "A novel prediction method based on the support vector regression for the remaining useful life of lithium-ion batteries," *Microelectron. Rel.*, vol. 85, pp. 99–108, Jun. 2018.

[74] K. Huang, K. Yao, Y. Guo, and Z. Lv, "State of health estimation of lithium-ion batteries based on fine-tuning or rebuilding transfer learning strategies combined with new features mining," *Energy*, vol. 282, Nov. 2023, Art. no. 128739.

[75] L. Yang, L. Zhao, X. Su, and S. Wang, "A lithium-ion battery RUL prognosis method using temperature changing rate," in *Proc. IEEE Int. Conf. Prognostics Health Manage. (ICPHM)*, Ottawa, ON, Canada, Jun. 2016, pp. 1–7.

[76] J. Xing, H. Zhang, and J. Zhang, "Remaining useful life prediction of—Lithium batteries based on principal component analysis and improved Gaussian process regression," *Int. J. Electrochem. Sci.*, vol. 18, no. 4, Apr. 2023, Art. no. 100048.

[77] H. Feng and D. Song, "A health indicator extraction based on surface temperature for lithium-ion batteries remaining useful life prediction," *J. Energy Storage*, vol. 34, Feb. 2021, Art. no. 102118.

[78] Z. Deng, X. Hu, P. Li, X. Lin, and X. Bian, "Data-driven battery state of health estimation based on random partial charging data," *IEEE Trans. Power Electron.*, vol. 37, no. 5, pp. 5021–5031, May 2022.

[79] J. Tian, R. Xiong, W. Shen, J. Lu, and X.-G. Yang, "Deep neural network battery charging curve prediction using 30 points collected in 10 min," *Joule*, vol. 5, no. 6, pp. 1521–1534, Jun. 2021.

[80] S. Jenu, A. Hentunen, J. Haavisto, and M. Pihlatie, "State of health estimation of cycle aged large format lithium-ion cells based on partial charging," *J. Energy Storage*, vol. 46, Feb. 2022, Art. no. 103855.

[81] S.-Z. Chen, Z. Liang, H. Yuan, L. Yang, F. Xu, and Y. Fan, "A novel state of health estimation method for lithium-ion batteries based on constant-voltage charging partial data and convolutional neural network," *Energy*, vol. 283, 2023, Art. no. 129103.

[82] Z. Meng, K. A. Agyeman, and X. Wang, "Multi-segment state of health estimation of lithium-ion batteries considering short partial charging," *IEEE Trans. Energy Convers.*, vol. 38, no. 3, pp. 1–11, Sep. 2023.

[83] S. Yang, C. Zhang, J. Jiang, W. Zhang, Y. Gao, and L. Zhang, "A voltage reconstruction model based on partial charging curve for state-of-health estimation of lithium-ion batteries," *J. Energy Storage*, vol. 35, Mar. 2021, Art. no. 102271.

[84] X. Feng, C. Weng, X. He, X. Han, L. Lu, D. Ren, and M. Ouyang, "Online state-of-health estimation for Li-ion battery using partial charging segment based on support vector machine," *IEEE Trans. Veh. Technol.*, vol. 68, no. 9, pp. 8583–8592, Sep. 2019.

[85] X. Xiong, Y. Wang, K. Li, and Z. Chen, "State of health estimation for lithium-ion batteries using Gaussian process regression-based data reconstruction method during random charging process," *J. Energy Storage*, vol. 72, Nov. 2023, Art. no. 108390.

[86] H. Meng, M. Geng, and T. Han, "Long short-term memory network with Bayesian optimization for health prognostics of lithium-ion batteries based on partial incremental capacity analysis," *Rel. Eng. Syst. Saf.*, vol. 236, Aug. 2023, Art. no. 109288.

[87] W. Shi, J. Cao, Q. Zhang, Y. Li, and L. Xu, "Edge computing: Vision and challenges," *IEEE Internet Things J.*, vol. 3, no. 5, pp. 637–646, Oct. 2016.

[88] J. Feng, W. Zhang, Q. Pei, J. Wu, and X. Lin, "Heterogeneous computation and resource allocation for wireless powered federated edge learning systems," *IEEE Trans. Commun.*, vol. 70, no. 5, pp. 3220–3233, May 2022.

[89] S. Li, H. He, Z. Wei, and P. Zhao, "Edge computing for vehicle battery management: Cloud-based online state estimation," *J. Energy Storage*, vol. 55, Nov. 2022, Art. no. 105502.

[90] X. Feng, X. Zhang, and Y. Xiang, "An inconsistency assessment method for backup battery packs based on time-series clustering," *J. Energy Storage*, vol. 31, Oct. 2020, Art. no. 101666.

[91] S. Jinlei, L. Wei, T. Chuanyu, W. Tianru, J. Tao, and T. Yong, "A novel active equalization method for series-connected battery packs based on clustering analysis with genetic algorithm," *IEEE Trans. Power Electron.*, vol. 36, no. 7, pp. 7853–7865, Jul. 2021.

[92] A. A. Pesaran, "Battery thermal models for hybrid vehicle simulations," *J. Power Sources*, vol. 110, no. 2, pp. 377–382, Aug. 2002.

[93] X. Peng, C. Ma, A. Garg, N. Bao, and X. Liao, "Thermal performance investigation of an air-cooled lithium-ion battery pack considering the inconsistency of battery cells," *Appl. Thermal Eng.*, vol. 153, pp. 596–603, May 2019.

[94] K. Fang, S. Chen, D. Mu, B. Wu, and F. Wu, "Investigation of nickel–metal hydride battery sorting based on charging thermal behavior," *J. Power Sour.*, vol. 224, pp. 120–124, Feb. 2013.

[95] W. Haiying, D. Kai, L. Gechen, and W. Feng, "Research on the consistency of the power battery based on multi-points impedance spectrum," in *Proc. Int. Forum Strategic Technol.*, Oct. 2010, pp. 1–4.

[96] X. Feng, C. Xu, X. He, L. Wang, S. Gao, and M. Ouyang, "A graphical model for evaluating the status of series-connected lithium-ion battery pack," *Int. J. Energy Res.*, vol. 43, no. 2, pp. 749–766, Feb. 2019.

[97] F. An, W. Zhang, B. Sun, J. Jiang, and X. Fan, "A novel battery pack inconsistency model and influence degree analysis of inconsistency on output energy," *Energy*, vol. 271, May 2023, Art. no. 127032.

[98] C. Zhang, Y. Jiang, J. Jiang, G. Cheng, W. Diao, and W. Zhang, "Study on battery pack consistency evolutions and equilibrium diagnosis for serial-connected lithium-ion batteries," *Appl. Energy*, vol. 207, pp. 510–519, Dec. 2017.

[99] B. Shi, Y. Zhang, C. Yuan, S. Wang, and P. Li, "Entropy analysis of short-term heartbeat interval time series during regular walking," *Entropy*, vol. 19, no. 10, p. 568, Oct. 2017.

[100] P. Wei and H.-X. Li, "Spatiotemporal entropy for abnormality detection and localization of Li-ion battery packs," *IEEE Trans. Ind. Electron.*, vol. 70, no. 12, pp. 1–9, Dec. 2023.

[101] X. Gu, J. Li, K. Liu, Y. Zhu, X. Tao, and Y. Shang, "A precise minor-fault diagnosis method for lithium-ion batteries based on phase plane sample entropy," *IEEE Trans. Ind. Electron.*, early access, Oct. 9, 2023.

[102] Y. Chen, X. Liu, Y. Cui, J. Zou, and S. Yang, "A multiwinding transformer cell-to-cell active equalization method for lithium-ion batteries with reduced number of driving circuits," *IEEE Trans. Power Electron.*, vol. 31, no. 7, pp. 4916–4929, Jul. 2016.

[103] Y. Chen, X. Liu, H. K. Fathy, J. Zou, and S. Yang, "A graph-theoretic framework for analyzing the speeds and efficiencies of battery pack equalization circuits," *Int. J. Electr. Power Energy Syst.*, vol. 98, pp. 85–99, Jun. 2018.

[104] X. Yang, Z. Li, T. Q. Zheng, X. You, and P. Kobrle, "Virtual impedance sliding mode control-based MMC circulating current suppressing strategy," *IEEE Access*, vol. 7, pp. 26229–26240, 2019.

[105] F. Errigo, L. De Oliveira Porto, and F. Morel, "Design methodology based on prebuilt components for modular multilevel converters with partial integration of energy storage systems," *Energies*, vol. 15, no. 14, p. 5006, Jul. 2022.

[106] T. Fang, S. Shen, Y. Jin, and X. Ruan, "Robustness investigation of multi-inverter paralleled grid-connected system with LCL-filter based on the grid-impedance allocation mechanism," *IEEE Trans. Power Electron.*, vol. 36, no. 12, pp. 14508–14524, Dec. 2021.

[107] J. Li, R. Li, and X. Ruan, "Resonance analysis of multiple grid-connected inverters' series and parallel network," *IET Renew. Power Gener.*, vol. 17, no. 5, pp. 1106–1118, Apr. 2023.

XIANGYANG XIA received the Ph.D. degree in power systems and automation from Hunan University, Changsha, China, in 2009. He is currently a Professor with the Department of Electrical Engineering, Changsha University of Science and Technology, Changsha. His current research interests include power electronic applications in power systems and energy storage security control.

JIAHUI YUE was born in Henan, China, in 1994. He received the B.S. and M.S. degrees in electric engineering from Xinjiang University, Xinjiang, China, in 2021. He is currently pursuing the Ph.D. degree with Changsha University of Science and Technology, Changsha, China. His research interests include energy storage data analysis and energy storage safety.

XIAOYONG ZENG (Member, IEEE) received the Ph.D. degree in control science and engineering from Central South University, Changsha, China, in 2018. He is currently a Lecturer with the College of Electrical and Information Engineering, Changsha University of Science and Technology, Changsha. His research interests include complex systems modeling and lithium-ion battery state estimation.

YUAN GUO was born in Hunan, China, in 1999. He received the B.S. degree from the Changsha University of Science and Technology, Changsha, China, in 2021, where he is currently pursuing the M.S. degree. His research interest includes energy storage data analysis.

YONGKAI XIA was born in Shandong, China, in 1999. He received the bachelor's degree in electrical engineering from North China University of Water Resources and Electric Power, in 2021. He is currently pursuing the master's degree with the Changsha University of Science and Technology, China. His research interest includes the state estimation of lithium batteries for electric vehicles.

CHONGGENG LV was born in Hunan, China, in 1999. He received the bachelor's degree in electrical engineering from Nanhua University, in 2021. He is currently pursuing the master's degree with Changsha University of Technology. His research interest includes energy storage safety and control.

GUIQUAN CHEN was born in Guangxi, China, in 1997. He received the B.S. degree in electric engineering from Changsha University of Science and Technology, Changsha, China, in 2020, where he is currently pursuing the Ph.D. degree. His research interest includes energy storage safety and control.

• • •